FINAL REPORT, JUNE 2026

Shifts in the distributions of Wyoming's vegetation communities, habitats, and bird and mammal Species of Greatest Conservation Need under future climate

Prepared for the Wyoming Game and Fish Department

Paige E. Copenhaver-Parry, Ian Abernethy, Bradley K. Parry, Melanie Arnett, Srivenkatesh Vasiraju, Shelby N. Byerly, and Morgan D.T. Frost
Wyoming Natural Diversity Database
University of Wyoming

ABSTRACT

Climate change is expected to re-organize and redistribute vegetation communities, with cascading impacts on faunal taxa that rely on the existing structure and configuration of vegetation. Current faunal distribution patterns reflect the hierarchical influences of climate and vegetation on habitat availability, habitat quality, and habitat selection, and understanding the quantitative associations between species and habitat is of fundamental importance for anticipating the effects of climate change on wildlife. To inform proactive wildlife and habitat management within Wyoming, we projected changes in the distributions of Wyoming's terrestrial vegetation communities, habitats, and bird and mammal Species of Greatest Conservation Need (SGCN) over the coming century. We jointly modeled the percent cover of 134 vascular plant species using Generalized Joint Attribute Modeling (GJAM) and classified predicted plant assemblages into 27 distinct terrestrial plant communities and nine terrestrial habitat types. Vegetation projections were generated for mid-century (2041–2070) and end-of-century (2071–2100) under two CMIP6 global climate models and two greenhouse gas emissions scenarios. Classified vegetation predictions were then introduced alongside direct climate and landscape predictors to model the distributions of 118 of Wyoming's bird and mammal SGCN, and future vegetation projections were used to drive bird and mammal models forward to the middle and end of the current century. Across modeled species, vegetation community was the single most important predictor of wildlife distributions, emphasizing the central role of habitat in shaping bird and mammal occurrence patterns. Model projections show marked westward expansions of plains grassland communities and grassland associated bird and mammal SGCN under future climate, accompanied by more modest westward contractions in sagebrush vegetation communities and sagebrush associated birds and mammals. Alpine bird and mammal SGCN are projected to decline under future climate in tandem with contractions in subalpine vegetation, while expansions in upper montane vegetation communities and contractions in lower montane communities contribute to variable climate change responses among montane bird and mammal SGCN. These vegetation-informed projections of potential changes in SGCN bird and mammal distributions under future climate clarify the links between climate-induced risks to Wyoming's wildlife and changes in primary habitat components, providing insights relevant to habitat management.

CITATION

Copenhaver-Parry, P.E., Abernethy, I., Parry, B.K., Arnett, M., Vasiraju, S., Byerly, S.N., & Frost, M.D.T. 2026. Shifts in the distributions of Wyoming's vegetation communities, habitats, and bird and mammal Species of Greatest Conservation Need under future climate. Report prepared for the Wyoming Game and Fish Department by the Wyoming Natural Diversity Database, University of Wyoming.

SUPPORTING INFORMATION

Appendix S1. Species-level model performance diagnostics for upland and wetland vegetation models.

Appendix S2. Vegetation community maps.

Appendix S3. Terrestrial habitat maps.

Appendix S4. Model performance diagnostics for bird and mammal SGCN models.

Appendix S5. Bird SGCN maps.

Appendix S6. Mammal SGCN maps.

AKNOWLEDGEMENTS

We are grateful to Zack Walker and Zach Wallace of the Wyoming Game and Fish Department for providing guidance and support for this effort. This project was funded by the Wyoming Game and Fish Department.

I. Introduction

Landscapes across the western U.S. are exhibiting early indicators of ecosystem transformations underpinned by climate change-induced re-organization and redistribution of vegetation communities, and many of these changes portend biodiversity declines (Feeley et al. 2020; Jackson 2021; Rosenblad et al. 2023). Such changes are expected to have cascading impacts on faunal taxa that rely on the existing structure and configuration of plant assemblages (e.g. Martin & Maron 2012) and, indeed, dramatic declines in the diversity and distributions of animals have already been observed (Dirzo et al. 2014). Vegetation is considered a primary component of animal habitat which, more broadly, encompasses the set of conditions, resources, and risks sufficient to enable the occurrence of a given species (Morris 2003; Northrup et al. 2022). Primary environmental resources including heat, light, water, and nutrients directly contribute to animal habitat through their influence on animal physiology, but also indirectly determine the occurrence and quality of key habitat conditions and resources via their impact on plant productivity and composition (Davey & Stockwell 1991; Mackey & Lindenmayer 2001). Current faunal distribution patterns reflect the hierarchical influence of climate and vegetation on habitat availability, habitat quality, and habitat selection, and understanding the quantitative associations between species and habitat is of fundamental importance for anticipating the effects of climate change on faunal taxa (Sohl 2014).

Species distribution models relate species occurrence data to environmental predictors and have been applied to describe the distributions of numerous animal species across the globe, including vertebrate taxa that occupy the Intermountain West (e.g., Waltari & Guralnick 2009; Knick et al. 2013; Stevens & Conway 2020) and Wyoming (e.g., Fedy et al. 2014; Abernethy 2025). Such studies have provided useful information on the critical drivers of species-habitat associations that can be used to inform habitat management (Winter et al. 2024). Habitats are a primary unit of conservation and the focus of many wildlife management activities. Yet, studies that project faunal distributions under future climate have provided information less relevant to habitat management because they predominantly rely on species-climate associations without consideration of more proximate and potentially manageable habitat variables such as vegetation (e.g., Lawler et al. 2009). This limitation reflects a lack of available projections of future changes in vegetation communities that can be used to drive animal species distribution models forward in time (Burdett et al. 2010).

Projecting changes in vegetation communities under future climate is complicated by the interspecific interactions that shape plant community composition and structure. The trajectory and pace of change in vegetation communities is determined in part by the individual responses of plant species to environmental change and by plant-plant interactions, which may modulate species-specific environmental responses to varying degrees depending on the nature and strength of interactions under particular environmental conditions (Clark et al. 2020). This ecological reality precludes modeling and projection of individual plant species with, for example, standard species distribution modeling approaches as a viable method with which to represent changes in habitat under future climate (Copenhaver-Parry et al. 2016). Advancements

in macroecological modeling through tools such as joint modeling have enabled simultaneous consideration of species-specific environmental responses and plant-plant interactions to produce probabilistic estimates of current and future community states (Nunez et al. 2022; Copenhaver-Parry & Byerly 2025), and such tools may be leveraged to better represent future habitat in projections of animal distributions.

Here, we combine joint modeling of 134 terrestrial plant species with formal vegetation classification to predict the current and future distributions of 27 terrestrial plant communities and 9 habitat types within Wyoming, then utilize vegetation projections in combination with direct climate drivers to model the current and future distributions of 40 mammal and 83 bird species of greatest conservation need (SGCN) that occupy Wyoming. This effort directly addresses an identified need to incorporate climate science into habitat management in Wyoming (WGFD 2017; WGFD 2025) and contributes information vital for conservation planning and decision making (Guisan et al. 2013; Stevens & Conway 2020). The specific objectives of this effort were to: (i) generate a cross-walk between US National Vegetation Classification groups and Wyoming State Wildlife Action Plan (SWAP) terrestrial habitat types to facilitate community-level vegetation modeling and projection at a scale relevant for habitat and species management; (ii) jointly model the abundance and distribution of a comprehensive suite of plant species occurring within Wyoming terrestrial habitat types, and project modeled communities and habitats under mid- and end-of-century climate in a manner that allows for shifts in the composition and configuration of vegetation communities over time; (iii) create distribution models for Wyoming's birds and mammal SGCN that consider vegetation and climate and project distributions under mid- and end-of-century climate; (iv) distribute data products through the Wyoming Natural Diversity Database's web applications to facilitate use in wildlife and habitat management.

II. Methods

2.1 Vegetation Modeling

2.1.1 Vegetation data

We modeled terrestrial vegetation communities using species percent cover data from the U.S. Forest Inventory and Analysis (FIA) database (Burrill et al. 2021) and the Assessment, Inventory, and Monitoring (AIM) database (US DOI Bureau of Land Management 2011), with additional wetland data compiled from existing WYNDD wetland datasets (Heidel & Laursen 2003; Tibbets et al. 2016a; Tibbets et al. 2016b; Washkoviak et al. 2018a; Washkoviak et al. 2018b). The most recent species percent cover records for all 1,552 Phase 2 FIA plots in Wyoming were extracted from the FIA database using the rFIA package (Stanke et al. 2020). Subplot estimates of cover by species were converted to plot estimates by taking the average of the cover estimates across all subplots. Terrestrial AIM plot species percent cover records and species lists were downloaded from the TerrADat geodatabase for the most recent survey of each

plot within Wyoming. At the suggestion of the Wyoming BLM AIM coordinator (J. Halperin), we removed from the dataset all plots in which tree cover equaled or exceeded 25%, owing to the low suitability of AIM field methods for describing forested conditions. Wetland AIM plot species percent cover and species lists were downloaded from the BLM AIM Riparian and Wetland Indicators hub for the most recent survey of each wetland plot within Wyoming. All plot records from FIA, AIM, and WYNDD datasets include full vegetation inventories, so species not present within plot inventory lists were treated as absent.

Exploratory model fits indicated the necessity of developing separate models for upland and wetland vegetation communities, so two separate datasets were compiled. Wetland FIA plots were separated from upland plots based on physiographic class codes. Terrestrial AIM and upland FIA datasets were compiled into a single dataset comprised of 1,157 vascular plant species across 3,679 plots (**Fig. 1**). We retained data for species occurring in at least 50 upland plots, leaving 133 vascular plant species across 3,679 upland plots. Wetland AIM, wetland FIA, and WYNDD wetland datasets were compiled into a single dataset comprised of 387 wetland plant species across 334 wetland plots (**Fig. 1**). We retained data for species occurring in at least 20 wetland plots, resulting in a final wetland dataset comprised of 57 vascular wetland plant species across 334 wetland plots. For wetland modeling, wetland data were aggregated with upland data to incorporate additional absence information for wetland species and to better constrain modeled responses.

Gridded contemporary and projected future climate data for the entirety of Wyoming were extracted from the CHELSA downscaled climate datasets at a 30 arc second spatial resolution (Karger et al. 2017). We calibrated models using contemporary climate data from the 1981-2010 normal period for 18 bioclimate variables. To project models under future climate, we utilized downscaled projections from CHELSA for two global climate models (GCMs) included in the Coupled Model Intercomparison Project Phase 6 (CMIP6; Eyring et al. 2016) and recommended under the Intersectoral Impact Model Intercomparison Project (ISIMIP3b; ISIMIP 2024): the GFDL-ESM4 model (Dunne et al. 2020) and the MPI-ESM1-2-HR model (Muller et al. 2018). For each model, we utilized projections for two shared socioeconomic pathways (SSP) representing both an optimistic scenario (SSP 1-2.6; 1.8°C warming by the end of the century) and a more plausible scenario (SSP 3-7.0; 3.6°C warming by the end of the century; IPCC 2021). Projections were made under all four GCM by SSP combinations to two future time periods: mid-century (2041-2070) and end-of-century (2071-2100).

We also considered additional environmental covariates that could be assumed to remain constant under future climate. We derived slope and aspect (transformed to northness by taking the cosine of the slope) from an 800-meter bare-earth digital elevation model (Mapzen 2022) using the elevatr and raster packages for R (Hijmans 2022; Hollister 2023). Topographic Wetness Index (TWI), which is a numeric index representing the tendency of an area to accumulate water based on slope and upslope draining area, was calculated from the DEM using the dynatop package in R (Smith & Metcalfe 2022). All topographic variables were resampled to the spatial resolution of the climate data. Surficial geology was considered as a categorical proxy for

substrate and was sourced from the 1:500,000 scale Surficial Geology Map of Wyoming (Case et al. 1998) and rasterized to the resolution of the climate data. Ecological region entered the models as a categorical predictor. We utilized the boundaries of the U.S. Environmental Protection Agency (EPA) Level III Ecoregions of the United States (US Environmental Protection Agency 2013) to define ecological regions.

2.1.2 Vegetation modeling and projection

We used the Generalized Joint Attribute Modeling framework (GJAM; Clark et al. 2017) to jointly model the percent cover of terrestrial plant species as a function of climate, topography, surficial geology, and ecological region. GJAM is a hierarchical Bayesian regression framework that utilizes a multivariate response distribution to fit a single model across multiple species. GJAM parameters include regression coefficients that describe the response of individual species to environmental covariates as well as a species covariance matrix, which captures correlations between species pairs. GJAM was selected for its ability to be fit on the community scale and to capture patterns arising from community processes, as well as its ability to accommodate continuous data types (i.e. percent cover; Clark et al. 2017). We developed separate GJAM models for upland and wetland vegetation.

For both upland and wetland datasets, species cover data for all target species were modeled in GJAM as continuous abundance (CA) data types and censored above 100 to correspond with the upper limit of percent cover data. The full datasets were split into calibration (75%) and validation (25%) sets using a stratified approach. We developed six candidate models for upland vegetation and seven candidate models for wetland vegetation representing different combinations of annual and seasonal climate covariates hypothesized to influence the composition and distributions of Wyoming's vegetation communities (**Table 1**) and limited collinearity by including only weakly correlated covariates (Pearson $r \leq |0.7|$) within the same model (Dormann et al. 2013). Each climate covariate set was expanded to include topographic covariates, a categorical ecological region predictor, quadratic terms for all continuous covariates and, in one case, a categorial surficial geology predictor. All continuous covariates were centered and scaled prior to model fitting. Models were fit using the gjam package in R (Clark et al. 2017) with default, regularizing priors and run for 20,000-30,000 iterations, with the first 50% of iterations discarded as burn-in. Convergence was confirmed by visual assessment of traceplots.

Candidate models were evaluated using the deviance information criterion (DIC; Gelman et al. 2004; **Table 1**) and the root mean square percent error (RMSPE) of in-sample and out-of-sample predictions for all modeled species (**Appendix S1**). Initial performance revealed overprediction of species with low prevalence. To eliminate species with insufficient specificity, we utilized a model discrimination criterion to filter additional species from the dataset. We calculated the True Skill Statistic (TSS; Allouche et al. 2006) by converting species cover predictions to presence/absence using the cover threshold that maximized the TSS for each species, then excluded from the dataset all species for which the maximum TSS did not reach or exceed 0.50 in at least one of the candidate models. This effort reduced the initial upland species

list to a set of 101 species, and the wetland species list to 33 species. The candidate GJAM models were then re-fit to the reduced set of species to produce a final set of candidate models for comparison. The model with the lowest DIC and not within two DIC units of another model was accepted as the best performing model and retained for validation, prediction, and mapping. We performed additional model evaluation using RMSPE values for each species (**Table S1.1**; **Table S1.2**) and the correspondence between observed and predicted values for both in-sample and out-of-sample predictions.

For many species, the final models poorly discriminated absences from very low percent cover. Accurate discrimination at low abundances is a recognized challenge in GJAM models (e.g., Scher et al. 2024; Copenhaver-Parry & Byerly 2025). To improve absence discrimination, we calculated absence thresholds for each species by applying Cohen's Kappa, a prevalence-dependent metric of model discrimination (Allouche et al. 2006). Prevalence-dependent model discrimination metrics have been argued to be more appropriate when the absolute values of the predictions are important, as is the case with our percent cover predictions (Lawson et al. 2014). We identified the cover threshold that maximized Kappa for each species (**Table S1.1**; **Table S1.2**) and then re-classified the predictions such that all values below the threshold were assigned a value of zero (absence), and all values equal to or exceeding the threshold retained their predicted percent cover values (Copenhaver-Parry & Byerly 2025).

Using the posterior distributions from the best models for upland and wetland vegetation, the percent cover of each focal species was predicted across all pixels within the study area under contemporary, mid-century and end-of-century climate across all four GCM by SSP scenarios. Predictions were generated at the resolution of the data: 30 arc seconds or approximately 1km^2.

2.1.3 Vegetation community classification and change

To evaluate projected changes at the community scale, we classified each mapped pixel to a particular terrestrial plant community type. We followed the U.S. National Vegetation Classification (USNVC 3.0) – a hierarchical vegetation classification widely used in the U.S. – to classify pixels to USNVC-defined "groups", which describe plant communities according to dominant, co-dominant, and other diagnostic species after accounting for regional and biogeographical distinctions (Faber-Langendoen et al. 2014). Using the type descriptions in the USNVC 3.0 catalog, we developed keys to assign USNVC group classifications to individual pixels based on the occurrence and relative cover of dominant, co-dominant, and diagnostic species as predicted from the best model. Because wetland species records were limited relative to upland records, we were unable to identify distinct wetland communities, and instead classified wetland pixels as a single wetland habitat type. Pixels were classified as wetland when the most abundant species predicted in a given pixel was a wetland obligate.

We further aggregated upland vegetation community predictions to the level of terrestrial habitats. Terrestrial habitats were defined consistent with the Wyoming State Wildlife Action Plan (SWAP; WGFD 2020). Using habitat descriptions within the SWAP, an existing crosswalk between SWAP habitats and Ecological Systems (WGFD 2020), and a crosswalk between

Ecological Systems and USNVC groups developed for USNVC 3.0 (Muldavin et al. 2025), we developed a new crosswalk to link USNVC defined vegetation communities occurring within Wyoming to terrestrial habitats (**Table 2**). This crosswalk extended beyond modeled communities to include USNVC groups that are understood to occur in Wyoming but were not sufficiently represented within our plot dataset. Using this crosswalk, mapped vegetation communities were aggregated to the habitat level under current climate and all future time periods and scenarios.

To evaluate changes in the extent of vegetation communities and habitats, we calculated the percent change in the area occupied by each community and habitat under future climate relative to contemporary climate. To summarize shifts in the distributions of vegetation communities and habitats under future climate, we calculated the mean location of community and habitat occurrences (hereafter referred to as community/habitat center of gravity) and calculated differences in centers of gravity between projections made under future climate scenarios and contemporary climate. To facilitate visualization and interpretation, we considered trends across communities grouped by ecological regions (plains, basins and foothills, mountains).

2.2 Bird and Mammal Species of Greatest Conservation Need Modeling

2.2.1 Bird and mammal data

We obtained occurrence records of 141 bird and mammal SGCN species (89 bird and 52 mammal taxa) from the Wyoming Biological Information System (WYBIS). This database is the most comprehensive source of Wyoming species occurrence records and includes data obtained from numerous sources including state and federal agencies, researchers, citizen scientists, and natural history museums, among others. Prior to modeling, we evaluated all occurrence records with system conflicts (e.g., out of range, unusual observation date, unrecognized activity for taxon, etc.) and removed all records with conflicts that could not be reconciled to ensure that erroneous occurrences were not included in models. Additionally, occurrences with a location error equal to or exceeding 3,000 m were removed due to lack of spatial precision. For all species, we limited observations to those collected between 1981 and 2024. For non-migratory birds and most mammals, we used year-round observations. For migratory and non-migratory bat species, we only retained observations made between June 1 and August 15 and June 1 and August 31, respectively. For migratory bird species, we limited observations to WYNDD's currently accepted reproductive period dates. Taxa with fewer than 22 occurrence locations after filtering were not modeled.

We considered 22 environmental predictors sourced from gridded datasets available at a 30 arc second spatial resolution. Predictors described climatic, hydrologic, vegetation, and other land cover influences on animal distributions (**Table 3**). Climate data were extracted from the CHELSA dataset as described in *2.1.1*. Vegetation community, predicted according to the methods in *2.1*, was introduced as a categorical predictor. We generated four topographic

variables derived from the National Elevation Dataset (U.S. Geological Survey 2018). To represent terrain heterogeneity, we calculated Topographic Ruggedness Index (TRI) for the modeling extent using the Riley method implemented using R package spatialEco (Riley et al. 1999; Evans 2026). We also represented cliffs, rocky outcrops, and cave features following the methods in Keinath et al. (2010).

Because water features influence the distribution of many wildlife species, we derived two hydrology variables that described the distance to permanent flowing or standing water features on the landscape. Specifically, we generated two predictor rasters that represent Euclidean distance to permanent surface-water features across Wyoming by filtering National Hydrography Dataset (NHD) vectors to permanent waterbody and flowline feature types, rasterizing those filtered vectors, and then computing cell-wise distance surfaces for permanent waterbodies and permanent flowlines (U.S. Geological Survey, National Geospatial Program 2023). To project future distance-to-water predictors, we applied simple warming-based scaling factors to existing baseline rasters for distance to permanent waterbodies and distance to permanent flowlines. For each of four climate scenarios we multiplied current distance values by a fixed factor of 5% increase in distance per 1° C in anticipated global warming for both mid-century and end-century temperature changes. Because models of changes in surface water under different climate change models and scenarios in Wyoming do not exist, this represents a proximate model using current NHD-derived distance to water surfaces under projected temperature increments.

All predictors were resampled to consistent projection, extent, and resolution using the terra package in R (Hijmans 2026). To minimize any potential influence of collinearity on transferability of MaxEnt models (Feng et al. 2019), we removed predictors with a correlation ≥ |0.70|, favoring removal of the variable with lower perceived biological relevance in each correlated pair (Dormann et al. 2013). We also omitted any predictor included in the vegetation community models from consideration as predictors in bird and mammal SGCN models. This resulted in a predictor set of nine variables for species that are associated with cliffs, rock outcrops, or caves and six variables for species that are not. Contemporary and projected future climate data used are described in detail above.

2.2.2 Bird and mammal modeling and projection

Models were generated using Maxent® version 3.4.3 implemented via the dismo package in R version 4.1.2 (Phillips et al. 2020; R Core Team 2024). Maxent is recognized as a robust algorithm for constructing species distribution models from opportunistically collected data, particularly when observations are sparse (Hijmans & Graham 2006; Graham et al. 2008; Wisz et al. 2008; Elith & Graham 2009). We applied the ‘ENMevaluate’ function in the ENMeval R package (Muscarella et al. 2014) to identify the feature response types and regularization multiplier values that minimized AIC for each species, then retained these values in model calibration (Laszlo et al. 2022). We generated a single set of 90,000 spatially balanced random background points weighted by the vegetation communities using the dismo R package (Valavi

et al. 2022) and utilized these points in all species models. Species distribution models were first fit from occurrence and background points using 10-fold cross-validation to generate continuous probability models under current conditions. For each species, we computed average model performance metrics including calibration AUC, validation AUC, AUC difference, and TSS (**Appendix S4**; Phillips et al. 2006; Phillips et al. 2017; Kass et al., 2025. To translate predicted occurrence probabilities to binary predictions of presence and absence, we applied the probability threshold that maximized TSS for each species (Liu et al. 2005).

Using response functions from MaxEnt models fit under contemporary climate conditions for each species, we predicted the probability of species occurrence under contemporary, mid-century, and end-of-century climate across all four CGM by SSP scenarios described in *2.1.1*.

2.2.3 Bird and mammal distribution shifts

To evaluate changes in the extent of predicted bird and mammal SGCN distributions in Wyoming, we calculated the percent change in the area occupied by each species under each future climate scenario relative to contemporary climate. To summarize shifts in the distributions of bird and mammal SGCN distributions under future climate, we calculated the mean center of gravity of bird and mammal distributions and calculated differences in centers of gravity between projections made under future climate scenarios and contemporary climate.

III. Results

3.1 Vegetation Model Performance

Of the six candidate GJAM models considering upland plant species, the best performing model included linear and quadratic effects of mean daily minimum air temperature of the coldest month (bio6), annual air temperature range (bio7), summer precipitation (bio18), winter precipitation (bio19), slope, aspect, topographic wetness index, and an ecological region effect (**Table 1**). This model minimized DIC and mean RMSPE relative to other candidate models and produced the best species-level performance (**Table S1.1**). The final model contained 1,919 estimated coefficients across 101 species. Each included coefficient was significant for at least 29 species ($\bar{x} = 57.736$, $s = 13.223$). RMSPE of species percent cover ranged from 0.635 to 4.058 ($\bar{x} = 1.032$, $s = 0.589$; **Table S1.1**). The model exhibited a tendency to underpredict percent cover, imposing a relatively consistent bias across all species. TSS and Kappa scores calculated on classified data confirm better-than-chance discrimination across all species (**Table S1.1**).

The best performing model of wetland plant species percent cover included linear and quadratic effects of the annual air temperature range (bio7), mean daily growing season temperature (bio10), winter precipitation (bio19), precipitation seasonality (bio15), slope, aspect, topographic wetness index, an ecological region effect, and a surficial geology effect (**Table 2**). This model minimized DIC relative to other candidate models and, despite demonstrating slightly larger mean RMSPE than other models, produced the best species-level performance

(**Table S1.2**). The final model contained 1,386 estimated coefficients across 33 species, with 714 coefficients estimated with significance. Species RMSPE ranged from 0.466% to 3.746% ($\bar{x} = 1.834\%$, $s = 1.010\%$; **Table S1.2**). TSS and Kappa scores confirm better-than-chance discrimination across all species ($\bar{x}_{TSS} = 0.617$; **Table S1.2**).

3.2 Geographic shifts in vegetation communities

Across all time periods and scenarios, the geographic extent of mountain communities declined, on average, to both the middle and end of the century (**Fig. 2**, **Fig. 3**, **Appendix S2**). Mountain communities occurring at lower elevation forest margins as well as those extending to upper treeline were projected to experience the most dramatic declines. In contrast, montane forest communities were projected to experience more modest, and often positive, changes in geographic extent. The decline in the extent of the Central Rocky Mountain Whitebark Pine-Subalpine Larch Forest and Woodland community exceeded the decline projected for any other vegetation community across all mid-century scenarios and for one end-of-century scenario (GFDL 1-2.6). End-of-century declines were predicted to be greatest for the Black Hills-Northwestern Great Plains Ponderosa Pine Forest and Woodland community (mountains) under scenario MPI 3-7.0, the Intermountain Semi-Desert Grassland community (basins and foothills) under scenario GFDL 3-7.0, and the Northern Great Plains Mesic Mixedgrass Prairie community (plains) under scenario MPI 1-2.6.

Declines in the extent of subalpine communities accompanied by moderate increases in montane community extent are consistent with other analyses within the U.S. Rocky Mountains that have projected subalpine tree species to experience severe reductions in suitable area over the coming century while montane forests and tree species increase in extent (Rehfeldt et al. 2006; Bell et al. 2014; Copenhaver-Parry et al. 2019). Subalpine communities are comprised of cool-adapted species with high sensitivity to warming (Ackerly et al. 2020) and will encounter reduced land area as they shift upslope (Elsen & Tingley 2015). Montane communities, in contrast, have more opportunity for upslope range shifts, particularly in the U.S. Rocky Mountains where land area increases toward mid-elevations (Elsen & Tingley 2015). Our projections indicate that the lowest elevation montane forest and woodland communities will be replaced by shrublands and grasslands along low elevation margins as they shift upslope, consistent with other model projections (Bell et al. 2014; Hansen & Phillips 2015; Copenhaver-Parry et al. 2019).

The geographic extent of plains communities was projected to increase, on average, in all but the MPI 1-2.6 scenario under end-of-century climate (**Fig. 2**, **Fig. 3**, **Appendix S2**). Under the remaining end-of-century projections and the MPI 3-7.0 mid-century projection, the Northern Great Plains Mesic Mixedgrass Prairie community was projected to increase in extent substantially more than any other vegetation community, expanding by more than 5000% under the higher emissions scenario. Changes in the geographic extent of individual plains communities were generally positive under both mid- and end-of-century climate, particularly for more mesic grassland communities. These projected changes are consistent with a widely

anticipated westward expansion of the Northern Great Plains ecoregional boundary as growing season precipitation increases (Easterling et al. 2017; Klemm et al. 2020). For plains forest and woodland communities, projected changes in extent tended to be more modest, or, in some cases, negative.

The geographic extent of basins and foothills communities increased, on average, across all scenarios and time periods, although several individual communities were projected to experience substantial declines in extent (**Fig. 2**, **Fig. 3**, **Appendix S2**). These projected changes largely reflect the incursion of plains grassland communities into sagebrush landscapes with increasing summer precipitation, as well as upslope expansions of foothills shrubland communities (**Fig. 2**). Sagebrush communities were projected to decline in extent in all scenarios. Yet, our species-specific model outputs for big sagebrush project only modest reductions in percent cover and extent under future climate, consistent with most projections of sagebrush within this ecoregion (Homer et al. 2015; Renwick et al. 2017; Rigge et al. 2021; Zimmer et al. 2020). Despite the relative persistence of sagebrush, graminoid cover is projected to increase substantially in areas currently occupied by sagebrush communities, shifting the community classification to a grassland type in many areas. Such projected increases in relative herbaceous cover and/or productivity across Wyoming basins in response to changing seasonal precipitation patterns are well supported by other studies (Zimmer et al. 2020; Rigge et al. 2021).

Intermountain Semi-Desert Grasslands were projected to experience almost complete loss by the end of the century under the higher emissions scenario and to decline in extent under all scenarios and time periods (**Fig. 2**, **Fig. 3**, **Appendix S2.22**), reflecting a considerable decline in the cold-adapted graminoids that define the community and a shift in community composition to favor salt desert shrubs. Salt desert shrub communities were consistently projected to increase in extent. Salt desert shrub communities already occupy the warmest and driest positions of the cold desert environmental gradient (Chambers et al. 2014) and are thus well positioned to benefit from future warming.

Across the higher emissions scenarios (3-7.0) under both GCMs and the low emissions scenario in the GFDL GCM (GFDL 1-2.6), plains communities were projected to experience the largest mean center of gravity shifts by mid-century, followed by basins and foothills communities and mountain communities (**Fig. 4**). Projections generated under the remaining scenario (MPI 1-2.6) demonstrated greater mean geographic shifts by mid-century for the basins and foothills communities. By the end of the century, all four scenarios projected basins and foothills communities to experience the largest mean geographic center of gravity shifts, followed by plains communities and mountain communities.

Under projected mid-century climate, vegetation communities showed diverse directional shifts in centers of gravity and there were limited trends apparent within and across ecological regions. By the end of the century, clearer directional patterns emerged although considerable variability remained (**Fig. 4**). Under projected end-of-century climate, plains communities generally shifted in more westerly directions, whereas the majority of mountain communities shifted in northwesterly directions. A smaller number of mountain communities showed distinct

eastward shifts. Projected shifts for basins and foothills communities were more variable; the largest shifts were projected to occur in southeasterly directions, but more groups shifted in westerly and northwesterly directions.

Such variable shifts likely reflect the physiographic influences of Wyoming's mountain ranges. Climate change in mountainous western regions has produced upslope temperature vectors and downslope moisture vectors and has not shifted consistently along latitudinal trajectories (Dobrowski et al. 2013). Indeed, most modeled communities were projected to shift upslope under future climate under all time periods and scenarios. Most of the few communities that were projected to shift downslope in alignment with moisture vectors are mesic communities (Northern Great Plains Mesic Forest and Woodland, North American Desert Alkaline-Saline Wet Scrub, Rocky Mountain-Interior Subalpine-Montane Aspen Forest, Southern Rocky Mountain Mesic-Moist Mixed Conifer Forest).

3.3 Geographic shifts in terrestrial habitats

Aggregating vegetation communities to the level of terrestrial habitats revealed emergent changes in the projected distributions of habitats under future climate (**Appendix S3**, **Fig. 5**). Across all time periods and scenarios, pronounced declines in geographic extent were projected for the Xeric and Lower Montane Forest habitat, Sagebrush Shrublands, and Mountain Grasslands. In all but the low emissions scenario under the GFDL GCM (GFDL 1-2.6), Montane and Subalpine Forest and Wetlands habitats were projected to decline in extent to the middle and end of the current century. In contrast, the geographic extent of Desert Shrublands and Prairie Grasslands habitats were projected to increase under all time periods and scenarios, and the Aspen/Deciduous Forest habitat and Foothills Shrublands habitat in all but one scenario each. Projected mean percent increases in geographic extent were largest for Desert Shrublands, which were projected to expand dramatically in area by the end of the century, followed by Foothills Shrublands. Projected percent losses in area were largest for Xeric and Lower Montane Forests, which were projected to contract by almost 90% in the most severe scenario, followed by Mountain Grasslands (**Fig. 5**).

Mean shifts in habitat centers of gravity (**Fig. 6**) were projected to be greatest for Xeric and Lower Montane Forests under mid-century and end-of-century climate, although shifts in Aspen/Deciduous Forests, Wetlands, and Foothills Shrublands exceeded those projected for Xeric and Lower Montane Forests in several individual scenarios. Xeric and Lower Montane Forests were projected to shift westward in all but the low emissions scenario under the MPI GCM projected to end-of-century climate; this center of gravity shift largely reflects a projected loss of Xeric and Lower Montane Forests in much of the eastern half of Wyoming (**Fig. S3.9**). Aspen/Deciduous Forests were projected to shift in a northerly direction, reflecting an expansion of this habitat type within the Greater Yellowstone Ecosystem (GYE; **Fig. S3.1**). Wetland centers of gravity were consistently projected to shift westward as wetland area declined in the Cheyenne watershed and the eastern portion of the North Platte watershed (**Fig. S3.8**). Directional shifts in Foothills Shrublands were inconsistent across scenarios (**Fig. S3.3**).

Sagebrush Shrublands were projected to shift their centers of gravity southwesterly across all time periods and scenarios, reflecting a decline in sagebrush community extent in the Bighorn Basin and the North Platte watershed (**Fig. 6**, **Fig. S3.7**). Habitat centers of gravity were projected to shift in northerly and northwesterly directions for both Mountain Grasslands and Montane and Subalpine Forests. These projected changes are underlain by projected declines in the Southern Rockies and persistence within the GYE (**Figs. S3.4**, **S3.5**). Finally, Prairie Grasslands were projected to shift westward, consistent with a projected westward expansion of plains communities with increasing growing season precipitation (**Figs. S3.6**).

3.4 Bird and mammal SGCN model performance

Of the 141 bird and mammal SGCN identified for modeling, we successfully modeled the distributions of 118 SGCN taxa (82 bird taxa and 36 mammal taxa; **Appendix S4**). For the remaining 23 SGCN, observations were too sparse ($n \leq 23$) to generate sufficient folds for cross-validation within the MaxEnt framework. Model performance diagnostics indicated good to strong discrimination between occurrence locations and background points across all modeled species (**Table S4.1**; **Table S4.2**). For SGCN birds, calibration AUC ranged from 0.710 for the Common Nighthawk (*Chordeiles minor*) to 0.999 for the Brown-capped Rosy-Finch (*Leucosticte australis*), with a median of 0.910. Validation statistics indicated relatively equivalent performance. For SGCN mammals, AUC ranged from 0.687 for the Plains Spotted Skunk (*Spilogale interrupta*) to 0.999 for the Pinon Deermouse (*Peromyscus truei*), with validation AUC averaging only 1.22 units lower across species. In general, visual inspection of binary model predictions suggests overprediction of occupied area for many species relative to the species' currently accepted range (e.g., Black-tailed Prairie Dog [*Cynomys ludovicianus*]; **Fig S6.5**). Yet, some species predictions are better constrained to the currently accepted range (e.g., Juniper Titmouse [*Baeolophus ridgwayi*]; **Fig. S5.13**).

Across all modeled species, vegetation community emerged as the most important predictor, with an average variable contribution of 23.61% (s = 19.88%). This was followed by the two direct climate predictors: bio10 (summer mean temperature; $\bar{x} = 22.54\%$, s = 19.31%) and annual precipitation (bio12; $\bar{x} = 19.39\%$, s = 17.88%). These three most important predictors accounted for approximately 65% of model contributions among all species. Landscape structure and hydrology predictors were important for a limited number of species but contributed modestly overall. The relative importance of predictors was broadly similar between birds and mammals

3.5 Geographic shifts in bird and mammal SGCN distributions

Across all climate scenarios to both the middle and end of the current century, both birds and mammals were projected to experience clear redistribution. Center of gravity shifts generally increased from mid-century to the end of the century (**Figs. 9-20**). Projections for SGCN birds showed mean center-of-gravity shifts ranging from 41.9 km (mid-century) to 46.2 km (end-century), averaged across all scenarios (**Figs. 9-14**), while mammals shifted from 38.0 km to

41.3 km over the same time periods (**Figs. 15-20**). Directional shifts were non-random and generally followed shifts in key vegetation communities and habitats driven by major climate change vectors. Most shifts for both bird and mammal SGCN were oriented northward and westward. Grassland-associated species were projected to experience the largest spatial displacements across both birds and mammals, generally exhibiting westward shifts (**Figs. 10, 18**).

Changes in occupied area were projected to be more heterogeneous. By the end of the century and averaged across all scenarios, mean geographic extent across bird SGCN increased by 9.8%; this projected expansion was driven primarily by grassland bird species (**Fig. 7**). Indeed, median change in geographic extent by the end of the century averaged across all scenarios was negative across all bird species ($\bar{x} =$ -0.7%), indicating a greater number of projected contractions than expansions. Grassland bird species were projected to experience a mean increase in area occupied of 14.2% averaged across all scenarios by the end of the century, achieved by expanding distributions westward by an average of 73.2 km (**Figs. 7, 10**). This pattern was consistent across most grassland birds but most pronounced among those currently restricted to eastern Wyoming such as Upland Sandpiper (*Bartramia longicauda*; **Fig. S5.14**). Some grassland species that are currently broadly distributed across Wyoming such as Thick-billed Longspur (*Rhynchophanes mccownii*; **Fig. S5.62**) and Short-eared Owl (*Asio flammeus*; **Fig S5.11**) were projected to decline in distributional extent.

Alpine bird SGCN were generally projected to shift their centers of gravity westward and northward and to experience contractions in occupied area, averaging 22.1% across all scenarios by the end of the century (**Figs. 7, 9**). However, the Brown-capped Rosy-Finch (*Leucosticte australis*) was projected to experience an increase in area occupied under all future climate scenarios and time periods (**Figs. 7, 9, S5.42**). Projected changes in montane bird distributions were more variable. On average, the area predicted to be suitable for montane bird species increased by 21.7% by the end of the century when averaged across all scenarios, and center of gravity shifts averaged 45.2 km (**Figs. 7, 11**). Most montane bird SGCN were projected to shift their centers of gravity in northwesterly directions; a smaller number were projected to shift eastward (**Fig. 11**).

Pinyon-juniper associated bird species were projected to experience highly variable directional shifts in their centers of gravity (**Fig. 12**). Projected changes in distributional extent were also variable (**Fig. 7**) with some species experiencing a projected increase in extent (e.g., Juniper Titmouse [*Baeolophus ridgwayi*]; **Fig. S5.13**) while others were projected to experience a decrease in extent (e.g., Bewick's Wren [*Thryomanes bewickii*]; **Fig. S5.73**). Most sagebrush associated bird species were projected to experience a mean westward center of gravity shift of 46.7 km by the end of the century when averaged across all scenarios (**Fig. 13**). In general, the distributional extents of individual sagebrush associated bird species were projected to decline by an average of 14.1% by the end of the century across all scenarios (**Fig. 7**), with the most severe declines projected for bird species considered sagebrush obligates such as Sagebrush Sparrow (*Artemisiospiza nevadensis*; **Fig. S5.10**) and Brewer's Sparrow (*Spizella breweri*; **Fig. S5.69**).

Finally, few trends were apparent in projected extents and directional shifts among water associated birds (**Figs. 7, 14**).

The distributions of SGCN mammals were projected to expand, on average across all scenarios, by the end of the century ($\bar{x} = 21.7\%$, $M = 8.1\%$), although mean change was largely driven by large projected expansions of bat species distributions. Across all SGCN bats, large directional shifts and expansions ($\bar{x} = 87.5\%$) were projected by the end of the century when averaged across all scenarios (**Figs. 8, 16**). These projected expansions reflect an increase in the extent of vegetation communities that are associated with many of Wyoming's bat SGCN but do not account for other critical pressures on bat populations, including White-nose syndrome (WNS). WNS is responsible for severe population declines in hibernating bat species, including the Little Brown Myotis (*Myotis lucifugus*), and regional populations are anticipated to continue to decline independent of future habitat changes (Frick et al. 2010; Cheng et al. 2021; Lile et al. in press).

Mammal SGCN that utilize alpine and sagebrush systems were generally projected to experience considerable contractions in geographic extent in association with contractions in subalpine and sagebrush vegetation communities. Alpine associated mammals were projected to experience small directional shifts ($\bar{x} = 9.5$ km by the end of the century, averaged across all scenarios), but large declines in geographic extent ($\bar{x} = 38.8\%$; **Figs. 8, 15).** Sagebrush associated SGCN mammals were projected to decline in extent by an average of 30.2% by the end of the century, averaged across all scenarios (**Fig. 8**), and to shift toward the north and west ($\bar{x} = 33.5$ km; **Figs. 8, 20**).

Consistent with the projected westward expansion of the Northern Great Plains ecological region, grassland associated mammals were projected to experience the largest center of gravity shifts, averaging 71.1 km by the end of the century averaged across all scenarios, mostly in a westerly direction (**Fig. 18**). Grassland associated mammals were projected to exhibit modest expansions and contractions in distributional extent ($\bar{x} = 3.5\%$; **Fig. 8**). Intermediate directional shifts in big-game species were projected with a mean center-of-gravity shift of 43.2 km by the end of the century averaged across all scenarios. Big game SGCN were projected to experience minimal changes in distributional extent with a mean change of -0.4% by the end of the century across all scenarios. Mule Deer (*Odocoileus hemionus*) were projected to increase in extent (**Fig. S6.25**) while Bighorn Sheep (*Ovis canadensis*; **Fig. S6.26**) and Moose (*Alces alces*; **Fig. S6.1**) distributions were projected to contract (**Figs. 8, 17**). Finally, montane associated mammal SGCN were projected to experience a slight average increase in extent of 7.3% by the end of the century averaged across all scenarios, accompanied by northward and westward center of gravity shifts averaging 30.0 km (**Figs. 8, 19**).

3.6 Data distribution in the WYNDD Data Explorer

To facilitate the use and application of these results, all vegetation community and habitat projections have been made available via the Wyoming Natural Diversity Database Data Explorer web application (https://wyndd.org/portal/apps/data_explorer/map). These new web

mapping services display spatial predictions of terrestrial vegetation communities and habitats at their native 30 arc-second resolution for current, mid-century- and end-of-century periods across all considered GCM and SSP combinations. Users can interact with projections directly within the web application via clickable identify features, by exploring mapped projections at a variety of zoom levels, by overlaying multiple projections to visualize change in communities and habitats over time, and by overlaying species observations to visualize spatial associations with recent observations of a variety of taxa. Rasterized projections with associated metadata are available for download directly within the web application. Similar functionality will soon be available for future projections of SGCN birds and mammals.

IV. Conclusions

Collectively, our results indicate that widespread redistribution of SGCN bird and mammal distributions in Wyoming is likely under future climate, and that climate-induced shifts in the vegetation communities that structure animal habitat will act as a primary proximate driver of distribution shifts. Many of the most dramatic changes we projected will occur among plains grassland communities and alpine and subalpine communities. Projected shifts in plains grassland communities correspond closely with an anticipated westward shift in the Northern Great Plains ecoregional boundary, driven by increasing growing season precipitation (Easterling et al. 2017; Klemm et al. 2020). In our results, this shift is evident in geographic expansions and westward shifts in plains grassland vegetation communities (**Figs. 2-4**), the prairie grasslands habitat (**Fig. 5, 6**), and in the majority of grassland associated bird and mammal SGCN (**Figs. 7, 8, 10, 18**).

Our results also highlight projected declines in the distributional extents of many sagebrush associated bird and mammal SGCN, occurring in association with a projected decline in the extent of sagebrush dominated vegetation communities (**Figs. 2, 3, 7, 8**). A decline in this vegetation type results from an increase in graminoid cover in Wyoming's basins and contractions of most sagebrush dominated communities toward the west. A projected increase in graminoid cover within sagebrush systems under changing seasonal precipitation is well supported (Zimmer et al. 2020; Rigge et al. 2021) and will alter habitat structure within Wyoming's basins. Yet, our species-level projections suggest that big sagebrush cover may decline only modestly across Wyoming's basins despite dramatic increases in graminoid cover. Because big sagebrush provides disproportionately critical wildlife cover and forage within this habitat (Beck et al. 2012), relative maintenance of sagebrush cover may give rise to more modest changes in sagebrush associated bird and mammal SGCN distributions than our projections indicate.

Our models project notable declines in the extent of subalpine vegetation communities and alpine bird and mammal SGCN (**Fig. 2, 3, 7, 8**). High elevation subalpine and alpine communities are comprised of cool-adapted species with high sensitivity to warming (Ackerly et al. 2020) and will encounter reduced land area as they shift upslope in concert with warming temperatures (Elsen & Tingley 2015). Montane communities, in contrast, have more opportunity

for upslope range shifts and may encounter increased land area as they shift upslope within the diamond-shaped ranges of the Rocky Mountains (Elsen & Tingley 2015). This will provide opportunities for variable shifts in the distributional extent of montane bird and mammal SGCN, consistent with our projections.

Taken together, our model projections confirm the overwhelming influence of vegetation – a key component of habitat – on the contemporary distributions of bird and mammal SGCN in Wyoming and demonstrate the value of vegetation community projections as inputs to animal distribution models. By providing vegetation-informed projections of potential changes in SGCN bird and mammal distributions under future climate, our findings clarify the links between climate-induced risks to Wyoming's wildlife and potentially manageable habitat variables, thereby providing information more directly useful for habitat management.

V. References

Abernethy, I. 2025. Distribution models for Wyoming's amphibian and reptile species of greatest conservation need. Report prepared for the Wyoming Game and Fish Department by the Wyoming Natural Diversity Database, University of Wyoming.

Ackerly, D.D., Kling, M.M., Clark, M.L., Papper, P., Oldfather, M.F., Flint, A.L., & Flint, L.E. 2020. Topoclimates, refugia, and biotic responses to climate change. Frontiers in Ecology and the Environment, 18(5): 288-297. https://doi.org/10.1002/fee.2204

Allouche, O., Tsoar, A., & Kadmon, R. 2006. Assessing the accuracy of species distribution models: Prevalence, Kappa and the True Skill Statistic (TSS). Journal of Applied Ecology, 43(6): 1223-1232. https://doi.org/10.1111/j.1365-2664.2006.01214.x

Beck, J.L., Connelly, J.W., & Wambolt, C.L. 2012. Consequences of treating Wyoming big sagebrush to enhance wildlife habitats. Rangeland Ecology and Management, 65: 4440455. https://doi.org/10.2111/REM-D-10-00123.1

Bell, D.M., Bradford, J.B., & Lauenroth, W.K. 2014. Mountain landscapes offer few opportunities for high-elevation tree species migration. Global Change Biology, 20: 1441-1451. https://doi.org/10.1111/gcb.12504

Burdett, C.L., Crooks, K.R., Theobald, D.M., Wilson, K.R., Boydston, E.E., Lyren, L.M., Fisher, R.N., Vickers, T.W., Morrison, S.A., & Boyce, W.M. 2010. Interfacing models of wildlife habitat and human development to predict the future distribution of puma habitat. Ecosphere, 1(1). https://doi.org/1890/ES10-00005.1

Burrill, E.A., DiTommaso, A.M., Turner, J.A., Pugh, S.A., Menlove, J., Christensen, G., Perry, C.J., & Conkling, B.L. 2021. The Forest Inventory and Analysis Database: Database description and user guide version 9.0.1 for Phase 2. U.S. Department of Agriculture, Forest Service.

Case, J.C., Arneson, C.S., & Hallberg, L.L. 1998. Preliminary 1:500,000-scale digital surficial geology map of Wyoming. Geological Hazards Section, Wyoming State Geological Survey, Laramie, WY.

Chambers, J.C., Bradley, B.A., Brown, C.S., D'Antonio, C., Germino, M.J., Grace, J.B., Hardegree, S.P., Miller, R.F., & Pyke, D.A. 2014. Resilience to stress and disturbance, and resistance to Bromus tectorum L. invasion in the cold desert shrublands of western North America. Ecosystems, 17: 360-375. https://doi.org/10.1007/s10020-013-9725-5

Cheng, T.L., Reichard, J.D., Coleman, J.T.H., Weller, T.J., Thogmartin, W.E., Reichert, B.E., Bennett, A.B., Broders, H.G., Campbell, J., Etchison, K., Feller, D.J., Geboy, R., Hemberger, T., Herzog, C., Hicks, A.C., Houghton, S., Humber, J., Kath, J.A., King, R.A., Loeb, S.C., Masse, A., Morris, K.M., Niderriter, H., Nordquist, G., Perry, R.W., Reynolds, R.J., Sasse, D.B., Scafini, M.R., Stark, R.C., Stihler, C.W., Thomas, S.C., Turner, G.G., Webb, S., Westrich, B.J., & Frick, W.F. 2021. The scope and severity of white-nose syndrome on hibernating bats in North America. Conservation Biology, 35(5): 1586-1597. https://doi.org/10.1111/cobi.13739.

Clark, J.S., Nemergut, D., Seyednasrollah, B., Turner, P., & Zhang, S. 2017. Generalized joint attribute modeling for biodiversity analysis: Median-zero, multivariate, multifarious data. Ecological Monographs, 87(1): 34–56. https://doi.org/10.1002/ecm.1241

Clark, J.S., Scher, C.L., & Swift, M. 2020. The emergent interactions that govern biodiversity change. Proceedings of the National Academy of Sciences, 117(29): 17074-17083. https://doi.org/10.1073/pnas.20038521147

Copenhaver-Parry, P.E. & Byerly, S.N. 2025. Joint model inference to support RAD-based decision making for aspen management in a changing climate. Canadian Journal of Forest Research, 55: 1-15. https://doi.org/10.1139/cjfr-2025-0244

Copenhaver-Parry, P.E., Albeke, S.E., & Tinker, D.B. 2016. Do community-level models account for the effects of biotic interactions? A comparison of community-level and species distribution modeling of Rocky Mountain conifers. Plant Ecology, 217: 533-547. https://doi.org/10.1007/s11258-016-0598-5

Copenhaver-Parry, P.E., Carroll, C.W., Martin, P.H., & Talluto, L. 2019. Multi-scale integration of tree recruitment and range dynamics in a changing climate. Global Ecology and Biogeography, 29(1): 102-116. https://doi.org/10.1111/geb.13012

Davey, S.M. & Stockwell, D.R.B. 1991. Incorporating wildlife habitat into an AI environment: concepts, theory, and practicalities. AI Applications, 5(2): 59-104. https://doi.org/10.5555/19950620129

Dirzo, R., Young, H.S., Galetti, M., Ceballos, G., Isaac, N.J.B., & Collen, B. 2014. Defaunation in the Anthropocene. Science, 345(6195): 401-406. https://doi.org/10.1126/science.1251817

Dobrowski, S.Z., Abatzoglou, J., Swanson, A.K., Greenberg, J.A., Mynsberge, A.R., Holden, Z.A., & Schwartz, M.K. 2013. The climate velocity of the contiguous United States during the 20th century. Global Change Biology, 19: 241-251. https://doi.org/10.1111/gcb.12026

Dormann, C.F., Elith, J., Bacher, S., Buchman, C., Carl, G., Carre, G., Carcia-Marquez, J.R., Gruber, B., Lafourcade, B., Leitao, P.J., Munkemuller, T., McClean, C., Osborne, P.E.,

Reineking, B., Schroder, B., Skidmore, A.K., Zurrell, D., & Lautenbach, S. 2013. Collinearity: A review of methods to deal with it and a simulation study evaluating their performance. Ecography, 36(1): 27–46. https://doi.org/10.1111/j.1600-0587.2012.07348.x

Dunne, J. P., Horowitz, L. W., Adcroft, A., Ginoux, P., Held, I. M., John, J. G., Krasting, J.P., Malyshev, S., Naik, V., Paulot, F., Shevliakova, E., Stock, C.A., Zadeh, N., Balaji, V., Blanton, C., Dunne, K.A., Dupuis, C., Durachta, J., Dussin, R., Gauthier, P.P.G., Griffies, S.M., Guo, H., Hallberg, R.W., Harrison, M., He, J., Hurlin, W., McHugh, C., Menzel, R., Milly, P.C.D., Nikonov, S., Paynter, D.J., Ploshay, J., Radhakrishnan, A., Rand, K., Reichl, B.G., Robinson, T., Schwarzkopf, D.M., Sentman, L.T., Underwood, S., Vahlenkamp, H., Winton, M., Wittenberg, A.T., Wyman, B., Zeny, Y., & Zhao, M. 2020. The GFDL Earth System Model Version 4.1 (GFDL-ESM 4.1): Overall coupled model description and simulation characteristics. Journal of Advances in Modeling Earth Systems, 12(11): e2019MS002015. https://doi.org/10.1029/2019MS002015

Easterling, D.R., Kunkel, K.E., Arnold, J.R., Knutson, T., LeGrande, A.N., Leung, L.R., Vose, R.S., Waliser, D.E., & Wehner, M.F. 2017. Precipitation change in the United States. In: D.J. Wuebbles, D.W. Fahey, K.A. Hibbard, D.J. Dokken, B.C. Stewart, & T.K. Maycock (Eds.). Climate science special report: fourth national climate assessment. U.S. Global Change Research Program, Washington, D.C., USA.

Elith, J. & Graham, C.H. 2009. Do they? How do they? WHY do they differ? On finding reasons for differing performances of species distribution models. Ecography, 32: 66-77. https://doi.org/10.1111/j.1600-0587.2008.05505.x

Elsen, P.R. & Tingley, M.W. 2015. Global mountain topography and the fate of montane species under climate change. Nature Climate Change, 5: 772-777. https://doi.org/10.1038/NCLIMATE2656

Evans, J. S. 2026. spatialEco: Spatial Analysis and Modelling Utilities. R package version 2.0-5. https://CRAN.R-project.org/package=spatialEco

Eyring, V., Bony, S., Meehl, G.A., Senior, C.A., Stevens, B., Stouffer, R.J., & Taylor, K.E. 2016. Overview of the coupled model intercomparison project phase 6 (CMIP6) experimental design and organization. Geoscience Model Development, 9(5): 1937–1958. https://doi.org/10.5194/gmd-9-1937-2016

Faber-Langendoen, D., Keeler-Wolf, T., Meidinger, D., Tart, D., Hoagland, B., Josse, C., Navarro, G., Ponomarenko, S., Saucier, J.-P., Weakley, A., & Comer, P. 2014. EcoVeg: A new approach to vegetation description and classification. Ecological Monographs, 84: 533-561. https://doi.org/10.1890-13-2334.1

Fedy, B.C., Doherty, K.E., Aldridge, C.L., O'Donnell, M., Beck, J.L., Bedrosian, B., Gummer, D., Holloran, M.J., Johnson, G.D., Kaczor, N.W., Kirol, C.P., Mandich, C.A., Marshall, D. McKee, G., Olson, C., Pratt, A.C., Swanson, C.C., & Walker, B.L. 2014. Habitat prioritization across large landscapes, multiple seasons, and novel areas: An example using Greater Sage-Grouse in Wyoming. Wildlife Monographs, 190: 1-39. https://doi.org/10.1002/wmon.1014

Feeley, K.J., Bravo-Avila, C., Fadrique, B., Perez, T.M., & Zuleta, D. 2020. Climate-driven changes in the composition of New World plant communities. Nature Climate Change, 10: 965-970. https://doi.org/10.1038/s41558-020-0873-2

Feng, X., Park, D.S., Liang, Y., Pandey, R., & Papes, M. 2019. Collinearity in ecological niche modeling: Confusions and challenges. Ecology and Evolution, 9(18): 10365-10376. https://doi.org/10.1002/ece3.5555

Frick, W.F., Pollock, J.F., Hicks, A.C., Langwig, K.E., Reynolds, D.S., Turner, G.G., Butchkoski, C.M., & Kunz, T.H. 2010. An emerging disease causes regional population collapse of a common North American bat species. Science, 329(5992): 679-682. https://doi.org/10.1126/science.1188594

Graham, C.H., Elith, J., Hijmans, R.J., Guisan, A., Townsend Peterson, A., Loiselle, B.A. & the NCEAS Predicting Species Distribution Working Group. 2008. The influence of spatial errors in species occurrence data used in distribution models. Journal of Applied Ecology, 45(1): 239-247. https://doi.org/10.1111/j.1365-2664.2007.01408.x

Guisan, A., Tingley, R., Baumgartner, J.B., Naujokaitis-Lewis, I., Sutcliffe, P.R., Tulloch, A.I.T., Regan, T.J., Brotons, L., McDonald-Madden, E., Mantyka-Pringle, C., Martin, T.G., Rhodes, J.R., Maggini, R., Setterfield, S.A., Elith, J., Schwartz, M.W., Wintle, B.A., Broennimann, O., Austin, M., Ferrier, S., Kearney, M.R., Possingham, H.P., & Buckley, Y.M. 2013. Predicting species distributions for conservation decisions. Ecology Letters 16(12): 1424-1435. https://doi.org/10.1111/ele.12189

Hansen, A.J. & Phillips, L.B. 2015. Which tree species and biome types are most vulnerable to climate change in the US Northern Rocky Mountains? Forest Ecology and Management, 228: 68-83. https://doi.org/10.1016/j.foreco.2014.11.008

Heidel, B. & Laursen, S. 2003. Botanical and ecological inventory of peatland sites on the Medicine Bow National Forest. Report prepared for Medicine Bow National Forest by Wyoming Natural Diversity Database, Laramie, WY.

Hijmans, R.J. & Graham, C.H. 2006. The ability of climate envelope models to predict the effect of climate change on species distributions. Global Change Biology, 12: 2272-2281. https://doi.org/10.1111/j.1365-2486.2006.01256.x

Hijmans, R.J. 2022. Raster: geographic data analysis and modeling. R package version 3.5-29. https://CRAN.R-project.org/package=raster

Hijmans, R.J. 2026. terra: Spatial Data Analysis. R package version 1.9-34. https://CRAN.R-project.org/package=terra

Hollister, J.W. 2023. elevatr: Access elevation data from various APIs. R package version 0.99.0. https://CRAN.R-project.org/package=elevatr/

Homer, C.G., Xian, G., Aldridge, C.L., Meyer, D.K., Loveland, T.R., & O'Donnell, M.S. 2015. Forecasting sagebrush ecosystem components and greater sage-grouse habitat for 2050: Learning from past climate patterns and Landsat imagery to predict the future. Ecological Indicators, 55: 131-145. https://doi.org/1-/1-16/j.ecolind.2015.03.002

IPCC. 2021. Climate Change 2021: The Physical Science Basis. Contribution of Working Group I to the Sixth Assessment Report of the Intergovernmental Panel on Climate Change [Masson-Delmotte, V., et al. (eds.)]. Cambridge University Press, Cambridge, United Kingdom and New York, NY, USA, 2391 pp. https://doi.org/10.1017/9781009157896.

ISIMIP. 2024. ISIMIP3b simulation protocol. Inter-Sectoral Impact Model Intercomparison Project. Available at: https://protocol.isimip.org/#/ISIMIP3b.

Jackson, S.T. 2021. Transformational ecology and climate change. Science, 373(6559): 1085-1086. https://doi.org/10.1126/scienceabj6777

Kass, J. M., Muscarella, R., Galante, P.J., Bohl, C., Buitrago-Pinilla, G.E., Boria, R.A., Soley-Guardia, M., & Anderson, R.P. 2025. ENMeval: Automated Tuning and Evaluations of Ecological Niche Models. R package version 2.0.5.2. https://CRAN.R-project.org/package=ENMeval

Keinath, D., Andersen, M., & Beauvais, G. 2010. Range and modeled distribution of Wyoming's species of greatest conservation need. Report prepared for the Wyoming Game and Fish Department by the Wyoming Natural Diversity Database, University of Wyoming.

Klemm, T., Briske, D.D., & Reeves, M.C. 2020. Potential natural vegetation and NPP responses to future climates in the U.S. Great Plains. Ecosphere, 11(10): e03264. https://doi.org/10.1002/ecs2.3264

Knick, S.T., Hanser, S.E., & Preston, K.L. 2013. Modeling ecological minimum requirements for distribution of greater sage-grouse leks: implications for population connectivity across their western range, USA. Ecology and Evolution, 3(6): 1539-1551. https://doi.org/10.1002/ece3.557

Laszlo, A.M., Placyk Jr., J.S., Williams, L.R., Williams, M.G., & Banta, J.A. 2022. A novel multivariate ecological approach to modeling freshwater mussel habitats verified by ground truthing. Hydrobiologia, 849: 3117-3133. https://doi.org/10.1007/s10750-022-04913-w

Lawler, J.J., Shafer, S.L., White, D., Kareiva, P., Maurer, E.P., Blaustein, A.R., & Bartlein, P.J. 2009. Projected climate-induced faunal change in the Western Hemisphere. Ecology, 90(3): 588-597. https://doi.org/10.1890/08-0823.1

Lawson, C.R., Hodgson, J.A., Wilson, R.J., & Richards, S.A. 2014. Prevalence, thresholds and the performance of presence-absence models. Methods in Ecology and Evolution, 5: 54-64. https://doi.org/10.1111/2041/210X.12123

Lile, R.E., Abernethy, I.M., Alston, J.M., Batie, D.P., Boodoo, L.C., Harrison, C., Olson, L., & Bernard, R.F. In press. Changes in summer bat captures in the Black Hills, South Dakota, after white-nose syndrome invasion. Journal of Mammalogy.

Liu, C., Berry, P.M., Dawson, T.P., & Pearson, R.G. 2005. Selecting thresholds of occurrence in the prediction of species distributions. Ecography, 28(3): 385-393. https://doi.org/10.1111/j.0906-7590.2005.03957.x

Mackey, B.G. & Lindenmayer, D.B. 2001. Towards a hierarchical framework for modeling the spatial distribution of animals. Journal of Biogeography, 28(9): 1147-1166. https://doi.org/10.1046/j.1365-2699.2001.00626.x

Mapzen. 2022. Terrain Tiles. Amazon Web Services. https://registry.opendata.aws/terrain-tiles.

Martin, T.E. & Maron, J.L. 2012. Climate impacts on bird and plant communities from altered animal-plant interactions. Nature Climate Change, 2: 195-200. https://doi.org/10.1038/nclimate1348

Morris, D.W. 2003. Toward an ecological synthesis: a case for habitat selection. Oecologia, 136: 1-13. https://doi.org/10.1007/s00442-003-1241-4

Muldavin, E., Faber-Langendoen, D., Davidson, A., & Conley, A. 2025. U.S. National Vegetation Classification 3.0: User Guide. Proceedings of the U.S. National Vegetation Classification, 8.

Muller, W.A., Jungclaus, J.H., Mauritsen, T., Baehr, J., Bittner, M., Budich, R., Bunzel, F., Esch, M., Ghosh, R., Haak, H., Ilyina, T., Kleine, T., Kornblueh, L., Li, H., Modali, K., Notz, D., Pohlmann, H., Roeckner, E., Stemmler, I., Tian, F., & Marotzke, J. 2018. A higher-resolution version of the Max Planck Institute Earth System Model (MPI-ESM1.2-HR). Journal of Advances in Modeling Earth Systems, 10: 1383-1413. https://doi.org/10.1029/20187MS001217

Muscarella, R., Galante, P.J., Soley-Guardia, M., Boria, R.A., Kass, J.M., Uriarte, M., & Anderson, R.P. 2014. ENMeval: An R package for conducting spatially independent evaluations and estimating optimal model complexity for MaxEnt ecological niche models. Methods in Ecology and Evolution, 5(11): 1198-1205. https://doi.org/10.1111/2041-210X.12261

Northrup, J.M., Vander Wal, E., Bonar, M., Fieberg, J., LaForge, M.P., LeClerc, M., Prokopenko, C.M., & Gerber, B.D. 2022. Conceptual and methodological advances in habitat-selection modeling: guidelines for ecology and evolution. Ecological Applications, 32(1): e02470. https://doi.org/10.1002/eap.2470

Nunez, C.L., Poulsen, J.R., White, L.J.T., Medjibe, V., & Clark. J.S. 2022. Distinct community-wide responses to forecasted climate change in Afrotropical forests. Frontiers in Ecology and Evolution, 9: 742626. https://doi.org/10.3389/fevo.2021.742626

Phillips, S. J., Anderson, R.P., & Schapire, R.E. 2006. Maximum entropy modeling of species geographic distributions. Ecological Modelling, 190(3): 231-259. https://doi.org/10.1016/j.ecolmodel.2005.03.026

Phillips, S.J., Dudik, M., & Schapire, R.E. 2017. Opening the black box: an open-source release of Maxent. Ecography, 40(7): 887-893. https://doi.org/10.1111/ecog.03049

Phillips, S.J., Dudik, M., & Schapire, R.E. 2020. Maxent softward for modeling species niches and distributions. R package version 3.4.3.

R Core Team. 2024. R: A language and environment for statistical computing. R Foundation for Statistical Computing, Vienna, Austria.

Rehfeldt, G.E., Crookston, N.L., Warwell, M.V., & Evans, J.S. 2006. Empirical analyses of plant-climate relationships for the western United States. International Journal of Plant Sciences, 167(6): 1123-1150. https://doi.org/10.1086/507711

Renwick, K.M., Curtis, C., Kleinhesselink, A.R., Schlaepfer, D., Bradley, B.A., Aldridge, C.L., Poulter, B., & Adler, P.B. 2017. Multi-model comparison highlights consistency in predicted effect of warming on a semi-arid shrub. Global Change Biology, 24: 424-438. https://doi.org/10.1111/gcb.13900

Riley, S. J., DeGloria, S. D., & Elliot, R. 1999. A terrain ruggedness index that quantifies topographic heterogeneity. Intermountain Journal of Sciences, 5: 23-27.

Rigge, M., Shi, H., & Postma, K. 2021. Projected change in rangeland fractional component cover across the sagebrush biome under climate change through 2085. Ecosphere, 12(6): e03538. https://doi.org/10.1002/ecs2.3538

Rosenblad, K.C., Baer, K.C., & Ackerly, D.D. 2023. Climate change, tree demography, and thermophilization in western US forests. Proceedings of the National Academy of Sciences, 120(18): e2301754120. https://doi.org/10.1073/pnas.2301754120

Scher, C.L., Roberts, S.M., Krause, K.P. & Clark, J.S. 2024. Leveraging relationships between species abundances to improve predictions and inform conservation. Journal of Applied Ecology, 61: 1662-1672. https://doi.org/10.1111/1365-2664.14670

Smith, P., and Metcalfe, P. 2022. Dynatop: An implementation of dynamic TOPMODEL hydrological model in R. R package version 0.2.3.

Sohl, T.L. 2014. The relative impacts of climate and land-use change on conterminous United States bird species from 2001 to 2075. PLoS ONE 9(11): e112251 https://doi.org/10.1371/journal.pone.0112251

Stanke, H., Finley, A.O., Weed, A.S., Walters, B.F., & Domke, G.M. 2020. rFIA: An R package for estimation of forest attributes with the US Forest Inventory and Analysis database. Environmental Modelling & Software, 127: 104664. https://doi.org/10.1016/j.envsoft.2020.104664

Stevens, B.S. & Conway, C.J. 2019. Mapping habitat suitability at range-wide scales: Spatially-explicit distribution models to inform conservation and research for marsh birds. Conservation Science and Practice 2(4): e178. https://doi.org/10.1111/csp2.178

Tibbets, T.M., Washkoviak, L., Tessmann, S., & Jones, G. 2016a. Wetland profile and condition assessment of the Goshen Hole Wetland Complex, Wyoming. Report prepared for the U.S. Environmental Protection Agency by The Nature Conservancy – Wyoming Chapter.

Tibbets, T.M., Washkoviak, L., Tessmann, S., & Jones, G. 2016b. Wetland profile and condition assessment of the Laramie Plains Wetland Complex, Wyoming. Report prepared for the U.S. Environmental Protection Agency by The Nature Conservancy – Wyoming Chapter.

U.S. DOI Bureau of Land Management. 2011. BLM Natl AIM TerrADat Hub. BLM Geospatial Business Platform National Hub Publisher. Updated 2023.

US Environmental Protection Agency. 2013. Level III ecoregions of the conterminous United States. U.S. EPA Office of Research and Development, Corvallis, OR.

U.S. Geological Survey. 2018. National Elevation Dataset, Version 2.0. U.S. Geological Survey, Reston, VA.

U.S. Geological Survey, National Geospatial Program. 2023. USGS National Hydrography Dataset Best Resolution (NHD) - Wyoming Shapefile. U.S. Geological Survey, Reston, VA.

Valavi, R., Guillera-Arroita, G., Lahoz-Monfort, J.J., & Elith, J. 2022. Predictive performance of presence-only species distribution models: a benchmark study with reproducible code. Ecological Monographs, 92(1): e01486. https://doi.org/10.1002/ecm.1486

Waltari, E. & Guralnick, R.P. 2009. Ecological niche modelling of montane mammals in the Great Basin, North America: examining past and present connectivity of species across basins and ranges. Journal of Biogeography, 36: 148-161. https://doi.org/10.1111/j.1365-2699.2008.01959.x

Washkoviak, L., Tibbets, T.M., & Jones, G. 2018a. Wetland profile and condition assessment of the Little Snake Wetland Complex, Wyoming. Report prepared for the U.S. Environmental Protection Agency by the Wyoming Natural Diversity Database, University of Wyoming.

Washkoviak, L., Tibbets, T.M., & Jones, G. 2018b. Wetland profile and condition assessment of the Great Divide Basin, Wyoming. Report prepared for the U.S. Environmental Protection Agency by the Wyoming Natural Diversity Database, University of Wyoming.

Winter, V.A., Smith, B.J., Berger, D.J., Hart, R.B., Huang, J., Manlove, K., Buderman, F.E., & Avgar, T. 2024. Forecasting animal distribution through individual habitat selection: insights for population inference and transferable predictions. Ecography: e07225. https://doi.org/10.1111/ecog.07225

Wisz, M.S., Hijmans, R.J., Li, J., Peterson, A.T., Graham, C.H., Guisan, A., & the NCEAS Predicting Species Distributions Working Group. 2008. Effects of sample size on the performance of species distribution models. Diversity and Distributions, 14(5): 763-773. https://doi.org/10.1111/j.1472-4642.2008.00482.x

Wyoming Game and Fish Department. 2017. State Wildlife Action Plan. https://wgfd.wyo.gov/wyoming-wildlife/wyoming-state-wildlife-action-plan

Wyoming Game and Fish Department. 2025. Statewide Habitat Plan. https://wgfd.wyo.gov/habitat/habitat-plans

Zimmer, S.N., Grosklos, G.J., Belmont, P., & Adler, P.B. 2020. Agreement and uncertainty among climate change impact models: A synthesis of sagebrush steppe vegetation projections. Rangeland Ecology and Management, 75(1): 1190129. https://doi.org/10.1016/j.rama.2020.12.006

VI. Tables

Table 1. Multiple candidate covariate sets were used to construct and fit generalized joint attribute models describing the percent cover of 101 terrestrial upland plant species and 33 wetland plant species. Standard bioclim variables were used to represent climatic influences and topographic effects were also considered, including topographic wetness index (TWI). Models were compared using the Deviance Information Criterion (DIC), the root mean square percent error (RMSPE) of individual species, and the mean RMSPE across all modeled species. The final selected models are indicated by gray shading.

Model	Covariates	Mean RMSPE	DIC
	Upland vegetation		
1	bio1, bio12, slope, aspect, TWI	3.85592	3115676
2	bio5, bio9, bio17, slope, aspect, TWI	3.84905	3068035
3	bio6, bio7, bio18, bio19, slope, aspect, TWI	3.83434	3018888
4	bio9, bio11, bio18, bio19, slope, aspect, TWI	3.84807	3027076
5	bio7, bio10, bio19, slope, aspect, TWI	3.85634	3041334
6	bio8, bio10, bio18, slope, aspect, TWI	3.83788	3025305
	Wetland vegetation		
1	bio1, bio12, slope, aspect, TWI	1.80841	1528589
2	bio7, bio10, bio19, slope, aspect, TWI	2.1335	1149169
3	bio7, bio10, bio19, bio15, slope, aspect, TWI	2.13129	1215288
4	bio7, bio10, bio19, bio15, slope, aspect, TWI, geology	2.08643	1146009
5	bio9, bio11, bio18, bio19, slope, aspect, TWI	1.80784	1482052
6	bio5, bio9, bio17, slope, aspect, TWI	1.81043	1472874
7	bio6, bio7, bio18, bio19, slope, aspect, TWI	2.13183	1228679

Table 2. Crosswalk of U.S. National Vegetation Classification vegetation groups to terrestrial habitats. Gray shading indicates modeled vegetation communities and habitats.

Habitat	U.S. National Vegetation Classification Group
Aspen/ Deciduous Forest	Great Plains Bur Oak Forest & Woodland
	Southern Rocky Mountain Mesic-Moist Mixed Conifer Forest
	Rocky Mountain-Interior Subalpine-Montane Aspen Forest
	Southern Rocky Mountain Gambel Oak - Mixed Montane Shrubland
Desert Shrublands	North American Desert Alkaline-Saline Wet Scrub
	Intermountain Semi-Desert Steppe & Shrubland
	Intermountain Dwarf Saltbush - Sagebrush Scrub
	Intermountain Shadscale - Saltbush Scrub
	Great Basin-Intermountain Ruderal Dry Shrubland & Grassland
	Great Plains Badlands Vegetation
Foothills Shrublands	Northern Great Plains Mesic Forest and Woodland
	Intermountain Basins Curl-leaf Mountain-mahogany Woodland and Scrub
	Central Rocky Mountain Montane-Foothill Shrubland
Montane and Subalpine Forest	Central Rocky Mountain Douglas-fir Mesic Forest
	Rocky Mountain Lodgepole Pine Forest & Woodland
	Rocky Mountain Subalpine Dry-Mesic Spruce - Fir Forest
	Central Rocky Mountain Whitebark Pine - Subalpine Larch Forest & Woodland
Mountain Grasslands	Central Rocky Mountain-Interior Montane Grassland & Meadow
	Central Rocky Mountain Lower Montane, Foothill & Valley Grassland
Prairie Grasslands	Northern Great Plains Dry Mixedgrass Prairie
	Northern Great Plains Mesic Mixedgrass Prairie
	Northern Great Plains Sand Prairie
	Northern & Central Great Plains Ruderal Grassland & Shrubland
	Intermountain Semi-Desert Grassland
Sagebrush Shrublands	Intermountain Low & Black Sagebrush Steppe & Shrubland
	Intermountain Basins Big Sagebrush Desert Shrubland
	Intermountain Basins Big Sagebrush Steppe
Wetlands	Rocky Mountain-Great Basin Swamp Forest
	Rocky Mountain Acidic Fen
	Rocky Mountain Alkaline Fen
	Arid West Interior Freshwater Marsh & Wet Meadow
	Vancouverian-Rocky Mountain Montane Wet Meadow & Marsh
	Vancouverian-Rocky Mountain Subalpine-Alpine Snowbed, Wet Meadow & Dwarf Shrubland
	Western North American Ruderal Marsh, Wet Meadow & Shrubland
	Great Plains Freshwater Marsh
	Great Plains Wet Meadow, Shrub Swamp & Seepage Fen
	Great Plains Playa & Rainwater Basin Wetland
	Great Plains Saline Wet Meadow & Marsh
	North American Desert Alkaline-Saline Marsh & Playa
Xeric and Lower Montane Forest	Southern Rocky Mountain Ponderosa Pine Forest & Woodland
	Central Rocky Mountain Ponderosa Pine Forest & Woodland
	Rocky Mountain Foothill-Rock Outcrop Limber Pine - Juniper Woodland
	Black Hills-Northwestern Great Plains Ponderosa Pine Forest & Woodland
	Rocky Mountain Montane-Subalpine Limber Pine Woodland
Riparian	Great Plains Cottonwood - Willow Floodplain Forest
	Rocky Mountain-Great Basin Montane Riparian Forest
	Central Rocky Mountain Lowland & Foothill Riparian Forest
	Western Arid Ruderal Lowland Riparian Forest & Scrub
	Rocky Mountain-Great Basin Lowland-Foothill Riparian Shrubland
	Western Montane-Subalpine Riparian & Seep Shrubland
Cliffs, Caves, Canyons, & Rock Outcrops	Intermountain Basins Cliff, Scree & Badland Sparse Vegetation
	Rocky Mountain & Sierran Alpine Bedrock & Scree
	Great Plains Cliff, Scree & Rock Vegetation
	Rocky Mountain Cliff, Scree & Rock Vegetation

Table 3. Climate, hydrology, landcover, and landscape structure variables used to represent climatic influences, surface water effects, habitat, and topographic effects in SGCN bird and mammal species at current, mid-century, and end-of-century time periods in Wyoming.

Variable	Description	Unit
bio10	Mean summer temperature	°C
bio12	Annual precipitation	millimeters
D_pf	Distance to any permanent flowing surface water feature	meters
D_pw	Distance to any permanent standing water feature	meters
Veg	Vegetation community	categorical
TRI	Topographic Roughness Index	ratio
D2cave	Distance to potentially cave-forming geologic formations	meters
D2cliffs	Distance to cliffs	meters
D2outcrop	Distance to rock outcrops	meters

VII. Figures

Figure 1. The focal area consists of the entire state of Wyoming within the western United States. We modeled upland terrestrial plant diversity using species percent cover data from 4,013 BLM AIM, USDA Forest Service FIA, and other wetland plots within Wyoming, and classified the region into three ecological regions based on EPA Level III ecoregions.

Figure 2. Mapped predictions of the distribution of terrestrial plant communities under contemporary climate (a) and projections under mid-century (b,c,d,e) and end-of-century (f,g,h,i) climate under two global climate models and two shared socioeconomic pathways representing a low emissions scenario (b,c,f,g) and a higher emissions scenario (d,e,h,i).

Figure 3. Projected percent change in the area occupied by all modeled terrestrial plant communities, grouped by ecological region, to mid- and end-of-century under two global climate models and two shared socioeconomic pathways.

Figure 4. The projected magnitude (km) and direction (degrees) of change in the geographic mean (center of gravity) for each modeled terrestrial plant community, colored according to ecological region, to mid-century (a,b,c,d) and end-of-century (e,f,g,h) under two global climate models and two shared socioeconomic pathways representing a low emissions scenario (a,b,e,f) and a higher emissions scenario (c,d,g,h).

Figure 5. Projected percent change in the area occupied by upland and wetland habitats to mid- and end-of-century under two global climate models and two shared socioeconomic pathways.

Figure 6. The projected magnitude (km) and direction (degrees) of change in the geographic mean (center of gravity) for each predicted terrestrial habitat to mid-century (a,b,c,d) and end-of-century (e,f,g,h) under two global climate models and two shared socioeconomic pathways representing a low emissions scenario (a,b,e,f) and a higher emissions scenario (c,d,g,h).

Figure 7. Projected percent change in the area occupied by all modeled SGCN birds, to mid- and end-of-century under two global climate models and two shared socioeconomic pathways.

Figure 8. Projected percent change in the area occupied by all modeled SGCN mammals to mid- and end-of-century under two global climate models and two shared socioeconomic pathways.

Figure 9. The projected magnitude (km) and direction (degrees) of change in the geographic mean (center of gravity) for each modeled alpine associated SGCN bird to mid-century and end-of-century under two global climate models and two shared socioeconomic pathways representing a low emissions scenario and a higher emissions scenario.

Figure 10. The projected magnitude (km) and direction (degrees) of change in the geographic mean (center of gravity) for each modeled grassland associated SGCN bird to mid-century and end-of-century under two global climate models and two shared socioeconomic pathways representing a low emissions scenario and a higher emissions scenario.

Figure 11. The projected magnitude (km) and direction (degrees) of change in the geographic mean (center of gravity) for each modeled montane forest associated SGCN bird to mid-century and end-of-century under two global climate models and two shared socioeconomic pathways representing a low emissions scenario and a higher emissions scenario.

Figure 12. The projected magnitude (km) and direction (degrees) of change in the geographic mean (center of gravity) for each modeled pinyon-juniper forest associated SGCN bird to mid-century and end-of-century under two global climate models and two shared socioeconomic pathways representing a low emissions scenario and a higher emissions scenario.

Figure 13. The projected magnitude (km) and direction (degrees) of change in the geographic mean (center of gravity) for each modeled sagebrush associated SGCN bird to mid-century and end-of-century under two global climate models and two shared socioeconomic pathways representing a low emissions scenario and a higher emissions scenario.

Figure 14. The projected magnitude (km) and direction (degrees) of change in the geographic mean (center of gravity) for each modeled wetland or water associated SGCN bird to mid-century and end-of-century under two global climate models and two shared socioeconomic pathways representing a low emissions scenario and a higher emissions scenario.

Figure 15. The projected magnitude (km) and direction (degrees) of change in the geographic mean (center of gravity) for each modeled alpine associated SGCN mammal to mid-century and end-of-century under two global climate models and two shared socioeconomic pathways representing a low emissions scenario and a higher emissions scenario.

Figure 16. The projected magnitude (km) and direction (degrees) of change in the geographic mean (center of gravity) for each modeled SGCN bat to mid-century and end-of-century under two global climate models and two shared socioeconomic pathways representing a low emissions scenario and a higher emissions scenario.

Figure 17. The projected magnitude (km) and direction (degrees) of change in the geographic mean (center of gravity) for each modeled SGCN big game species to mid-century and end-of-century under two global climate models and two shared socioeconomic pathways representing a low emissions scenario and a higher emissions scenario.

Figure 18. The projected magnitude (km) and direction (degrees) of change in the geographic mean (center of gravity) for each modeled grassland associated SGCN mammal to mid-century and end-of-century under two global climate models and two shared socioeconomic pathways representing a low emissions scenario and a higher emissions scenario.

Figure 19. The projected magnitude (km) and direction (degrees) of change in the geographic mean (center of gravity) for each modeled montane forest associated SGCN mammal to mid-century and end-of-century under two global climate models and two shared socioeconomic pathways representing a low emissions scenario and a higher emissions scenario.

Figure 20. The projected magnitude (km) and direction (degrees) of change in the geographic mean (center of gravity) for each modeled sagebrush associated SGCN mammal to mid-century and end-of-century under two global climate models and two shared socioeconomic pathways representing a low emissions scenario and a higher emissions scenario.

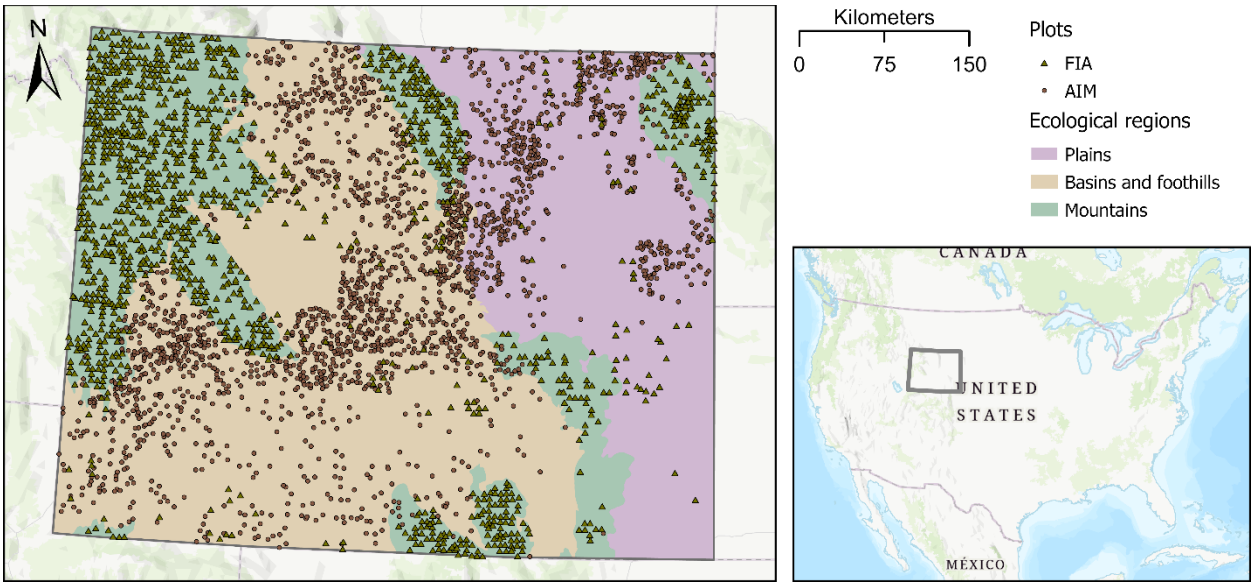
N
Kilometers
0
75
150
Plots
FIA
AIM
Ecological regions
Plains
Basins and foothills
Mountains
CANADA
UNITED
STATES
MÉXICO

Figure 1.

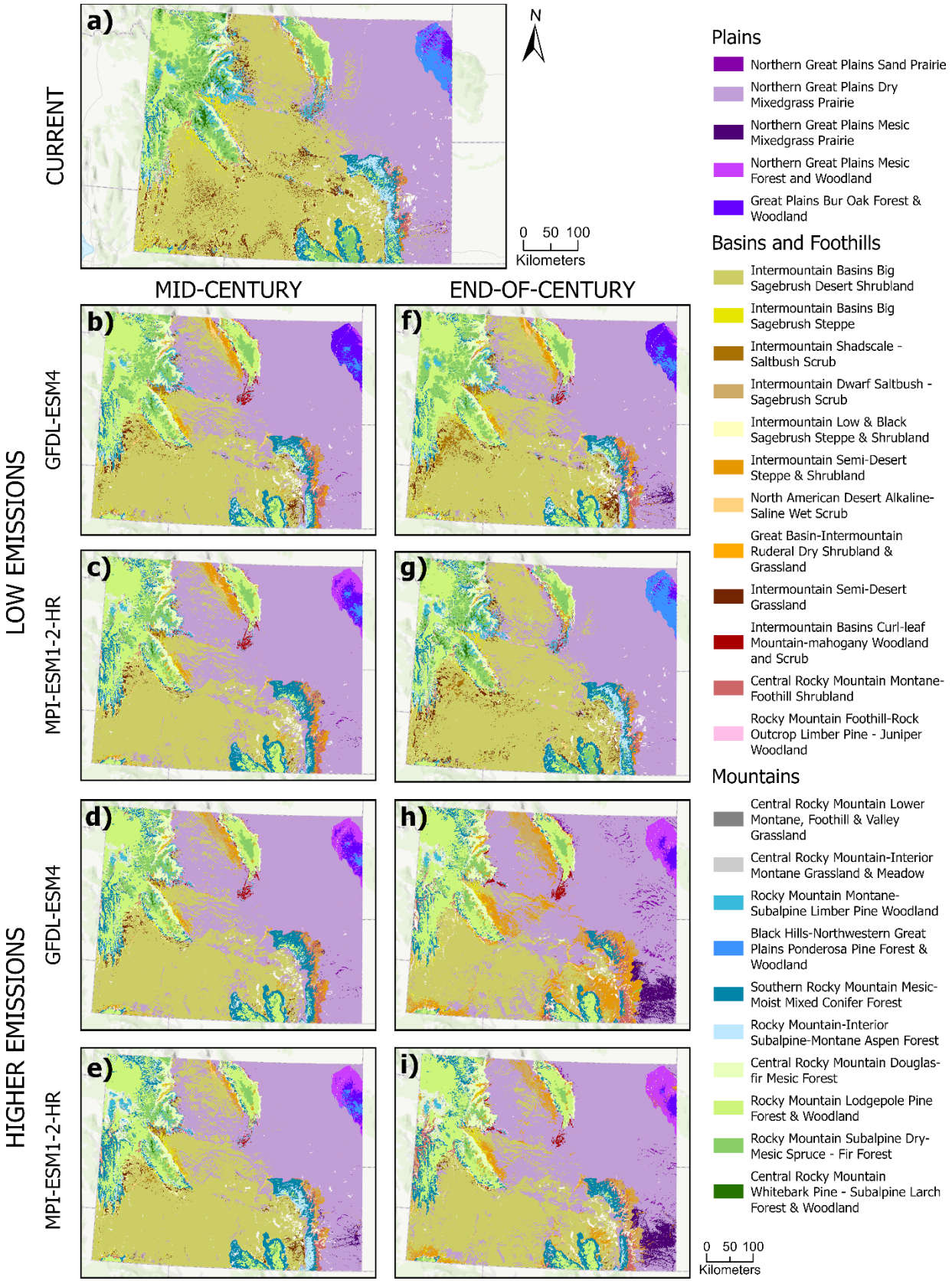
a)
CURRENT
N
0 50 100
Kilometers
MID-CENTURY
END-OF-CENTURY
LOW EMISSIONS
HIGHER EMISSIONS
GFDL-ESM4
MPI-ESM1-2-HR
GFDL-ESM4
MPI-ESM1-2-HR
b)
f)
c)
g)
d)
h)
e)
i)
Plains
Northern Great Plains Sand Prairie
Northern Great Plains Dry Mixedgrass Prairie
Northern Great Plains Mesic Mixedgrass Prairie
Northern Great Plains Mesic Forest and Woodland
Great Plains Bur Oak Forest & Woodland
Basins and Foothills
Intermountain Basins Big Sagebrush Desert Shrubland
Intermountain Basins Big Sagebrush Steppe
Intermountain Shadscale - Saltbush Scrub
Intermountain Dwarf Saltbush - Sagebrush Scrub
Intermountain Low & Black Sagebrush Steppe & Shrubland
Intermountain Semi-Desert Steppe & Shrubland
North American Desert Alkaline-Saline Wet Scrub
Great Basin-Intermountain Ruderal Dry Shrubland & Grassland
Intermountain Semi-Desert Grassland
Intermountain Basins Curl-leaf Mountain-mahogany Woodland and Scrub
Central Rocky Mountain Montane-Foothill Shrubland
Rocky Mountain Foothill-Rock Outcrop Limber Pine - Juniper Woodland
Mountains
Central Rocky Mountain Lower Montane, Foothill & Valley Grassland
Central Rocky Mountain-Interior Montane Grassland & Meadow
Rocky Mountain Montane-Subalpine Limber Pine Woodland
Black Hills-Northwestern Great Plains Ponderosa Pine Forest & Woodland
Southern Rocky Mountain Mesic-Moist Mixed Conifer Forest
Rocky Mountain-Interior Subalpine-Montane Aspen Forest
Central Rocky Mountain Douglas-fir Mesic Forest
Rocky Mountain Lodgepole Pine Forest & Woodland
Rocky Mountain Subalpine Dry-Mesic Spruce - Fir Forest
Central Rocky Mountain Whitebark Pine - Subalpine Larch Forest & Woodland
0 50 100
Kilometers

Figure 2.

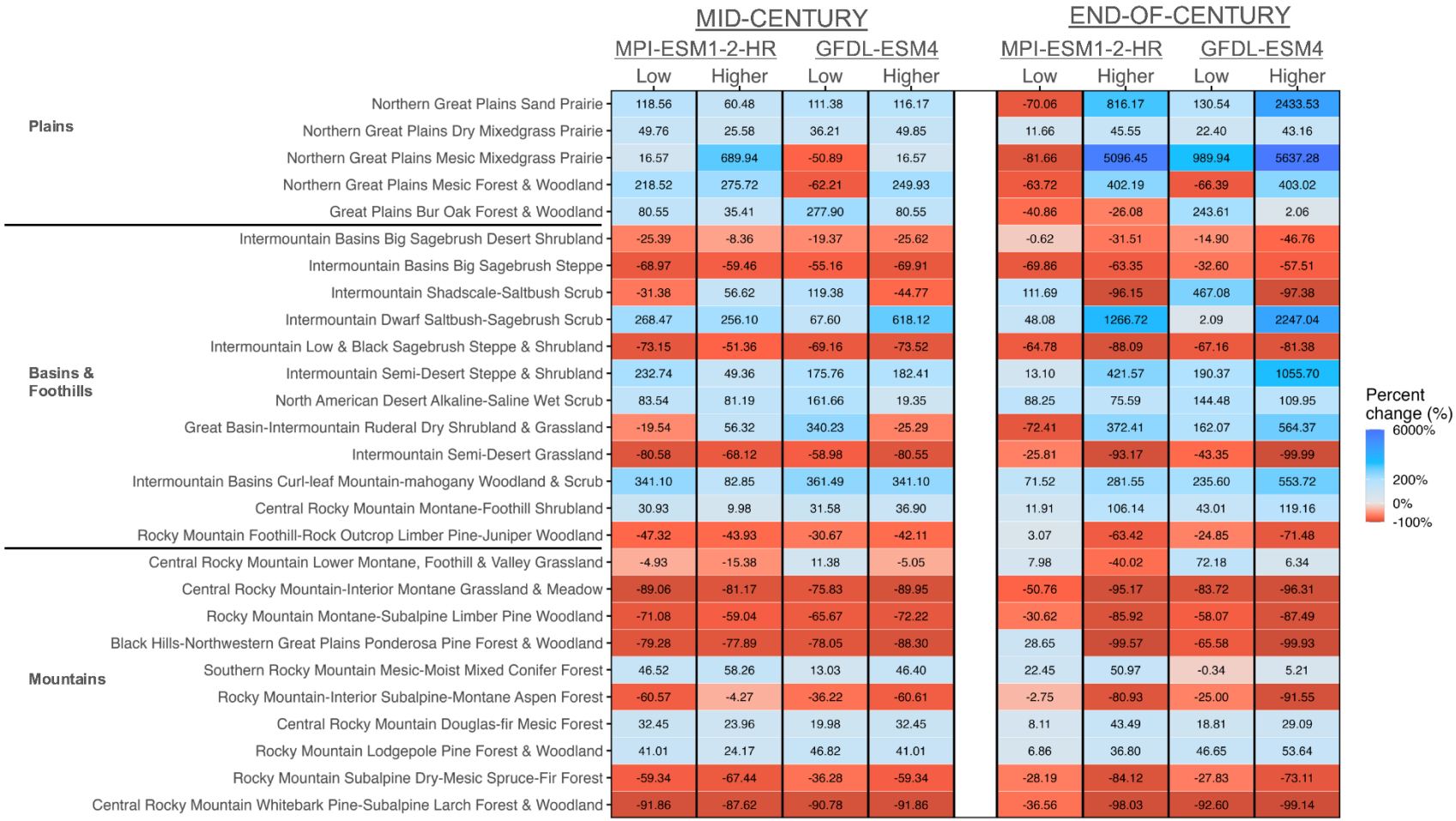
MID-CENTURY
END-OF-CENTURY
MPI-ESM1-2-HR
GFDL-ESM4
MPI-ESM1-2-HR
GFDL-ESM4
Low
Higher
Low
Higher
Low
Higher
Low
Higher
Plains
Northern Great Plains Sand Prairie 118.56 60.48 111.38 116.17 -70.06 816.17 130.54 2433.53
Northern Great Plains Dry Mixedgrass Prairie 49.76 25.58 36.21 49.85 11.66 45.55 22.40 43.16
Northern Great Plains Mesic Mixedgrass Prairie 16.57 689.94 -50.89 16.57 -81.66 5096.45 989.94 5637.28
Northern Great Plains Mesic Forest & Woodland 218.52 275.72 -62.21 249.93 -63.72 402.19 -66.39 403.02
Great Plains Bur Oak Forest & Woodland 80.55 35.41 277.90 80.55 -40.86 -26.08 243.61 2.06
Basins & Foothills
Intermountain Basins Big Sagebrush Desert Shrubland -25.39 -8.36 -19.37 -25.62 -0.62 -31.51 -14.90 -46.76
Intermountain Basins Big Sagebrush Steppe -68.97 -59.46 -55.16 -69.91 -69.86 -63.35 -32.60 -57.51
Intermountain Shadscale-Saltbush Scrub -31.38 56.62 119.38 -44.77 111.69 -96.15 467.08 -97.38
Intermountain Dwarf Saltbush-Sagebrush Scrub 268.47 256.10 67.60 618.12 48.08 1266.72 2.09 2247.04
Intermountain Low & Black Sagebrush Steppe & Shrubland -73.15 -51.36 -69.16 -73.52 -64.78 -88.09 -67.16 -81.38
Intermountain Semi-Desert Steppe & Shrubland 232.74 49.36 175.76 182.41 13.10 421.57 190.37 1055.70
North American Desert Alkaline-Saline Wet Scrub 83.54 81.19 161.66 19.35 88.25 75.59 144.48 109.95
Great Basin-Intermountain Ruderal Dry Shrubland & Grassland -19.54 56.32 340.23 -25.29 -72.41 372.41 162.07 564.37
Intermountain Semi-Desert Grassland -80.58 -68.12 -58.98 -80.55 -25.81 -93.17 -43.35 -99.99
Intermountain Basins Curl-leaf Mountain-mahogany Woodland & Scrub 341.10 82.85 361.49 341.10 71.52 281.55 235.60 553.72
Central Rocky Mountain Montane-Foothill Shrubland 30.93 9.98 31.58 36.90 11.91 106.14 43.01 119.16
Rocky Mountain Foothill-Rock Outcrop Limber Pine-Juniper Woodland -47.32 -43.93 -30.67 -42.11 3.07 -63.42 -24.85 -71.48
Mountains
Central Rocky Mountain Lower Montane, Foothill & Valley Grassland -4.93 -15.38 11.38 -5.05 7.98 -40.02 72.18 6.34
Central Rocky Mountain-Interior Montane Grassland & Meadow -89.06 -81.17 -75.83 -89.95 -50.76 -95.17 -83.72 -96.31
Rocky Mountain Montane-Subalpine Limber Pine Woodland -71.08 -59.04 -65.67 -72.22 -30.62 -85.92 -58.07 -87.49
Black Hills-Northwestern Great Plains Ponderosa Pine Forest & Woodland -79.28 -77.89 -78.05 -88.30 28.65 -99.57 -65.58 -99.93
Southern Rocky Mountain Mesic-Moist Mixed Conifer Forest 46.52 58.26 13.03 46.40 22.45 50.97 -0.34 5.21
Rocky Mountain-Interior Subalpine-Montane Aspen Forest -60.57 -4.27 -36.22 -60.61 -2.75 -80.93 -25.00 -91.55
Central Rocky Mountain Douglas-fir Mesic Forest 32.45 23.96 19.98 32.45 8.11 43.49 18.81 29.09
Rocky Mountain Lodgepole Pine Forest & Woodland 41.01 24.17 46.82 41.01 6.86 36.80 46.65 53.64
Rocky Mountain Subalpine Dry-Mesic Spruce-Fir Forest -59.34 -67.44 -36.28 -59.34 -28.19 -84.12 -27.83 -73.11
Central Rocky Mountain Whitebark Pine-Subalpine Larch Forest & Woodland -91.86 -87.62 -90.78 -91.86 -36.56 -98.03 -92.60 -99.14
Percent change (%)
6000%
200%
0%
-100%

Figure 3.

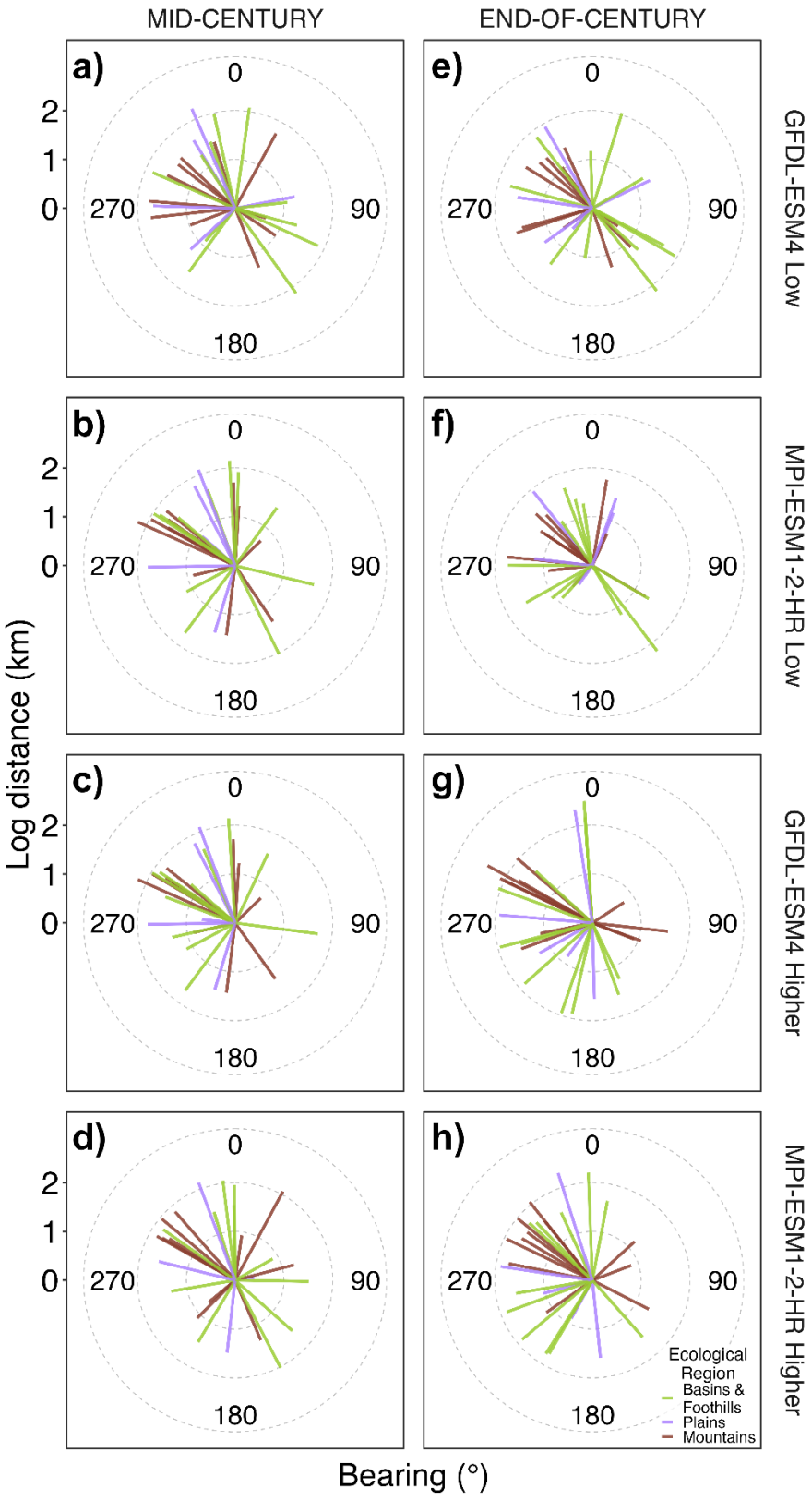
MID-CENTURY
END-OF-CENTURY
a)
b)
c)
d)
e)
f)
g)
h)
0
90
180
270
2
1
0
GFDL-ESM4 Low
MPI-ESM1-2-HR Low
GFDL-ESM4 Higher
MPI-ESM1-2-HR Higher
Log distance (km)
Bearing (°)
Ecological Region
Basins & Foothills
Plains
Mountains

Figure 4.

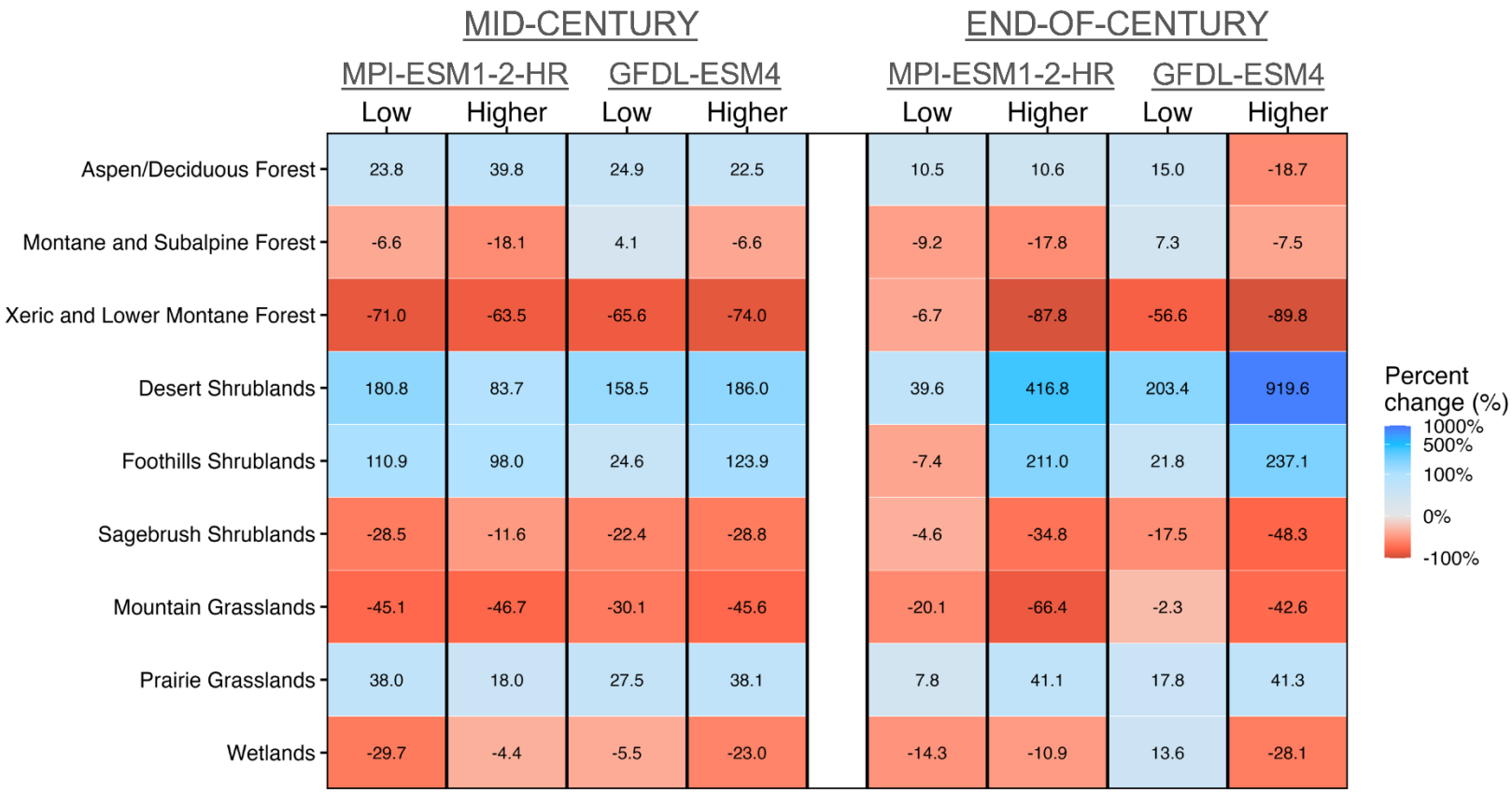
MID-CENTURY
END-OF-CENTURY
MPI-ESM1-2-HR
GFDL-ESM4
MPI-ESM1-2-HR
GFDL-ESM4
Low
Higher
Low
Higher
Low
Higher
Low
Higher
Aspen/Deciduous Forest
23.8 39.8 24.9 22.5 10.5 10.6 15.0 -18.7
Montane and Subalpine Forest
-6.6 -18.1 4.1 -6.6 -9.2 -17.8 7.3 -7.5
Xeric and Lower Montane Forest
-71.0 -63.5 -65.6 -74.0 -6.7 -87.8 -56.6 -89.8
Desert Shrublands
180.8 83.7 158.5 186.0 39.6 416.8 203.4 919.6
Foothills Shrublands
110.9 98.0 24.6 123.9 -7.4 211.0 21.8 237.1
Sagebrush Shrublands
-28.5 -11.6 -22.4 -28.8 -4.6 -34.8 -17.5 -48.3
Mountain Grasslands
-45.1 -46.7 -30.1 -45.6 -20.1 -66.4 -2.3 -42.6
Prairie Grasslands
38.0 18.0 27.5 38.1 7.8 41.1 17.8 41.3
Wetlands
-29.7 -4.4 -5.5 -23.0 -14.3 -10.9 13.6 -28.1
Percent change (%)
1000%
500%
100%
0%
-100%

Figure 5.

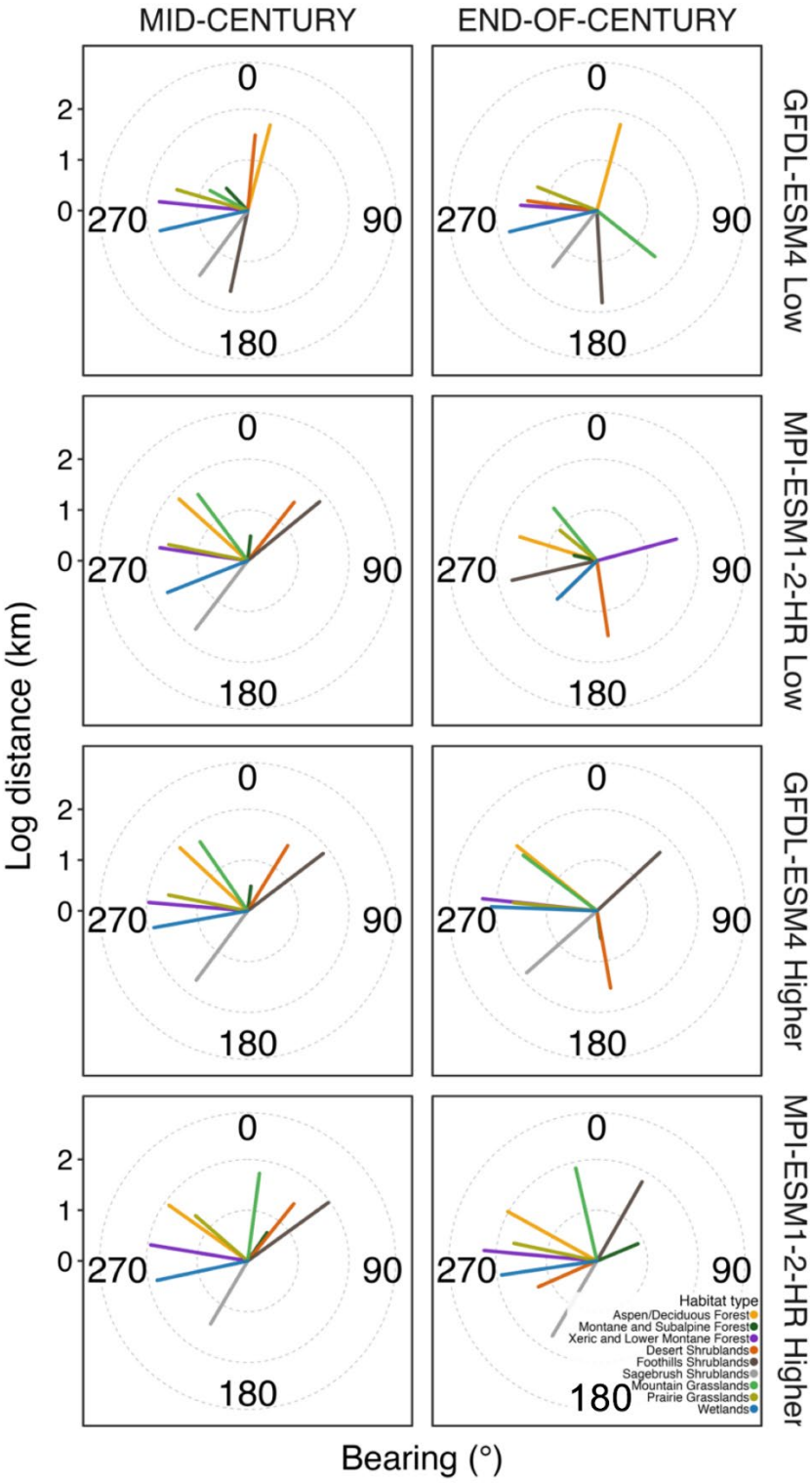
MID-CENTURY
END-OF-CENTURY
GFDL-ESM4 Low
MPI-ESM1-2-HR Low
GFDL-ESM4 Higher
MPI-ESM1-2-HR Higher
Log distance (km)
Bearing (°)
0
90
180
270
2
1
0
Habitat type
Aspen/Deciduous Forest
Montane and Subalpine Forest
Xeric and Lower Montane Forest
Desert Shrublands
Foothills Shrublands
Sagebrush Shrublands
Mountain Grasslands
Prairie Grasslands
Wetlands

Figure 6.


MID-CENTURY
END-OF-CENTURY
MPI-ESM1-2-HR
GFDL-ESM4
Low
High
Clark's Grebe (Aechmophorus clarkii) 1.9 6.7 2.3 4.3 4.5 3.7 4.4 2.4
Western Grebe (Aechmophorus occidentalis) 62.6 180.4 76.7 204.0 72.1 287.0 77.4 266.8
Boreal Owl (Aegolius funereus) -2.7 -12.1 2.9 -8.3 -4.0 -28.2 3.3 -16.1
Grasshopper Sparrow (Ammodramus savannarum) 10.7 -2.4 17.9 9.4 -2.5 1.6 12.9 7.7
Mountain Plover (Anarhynchus montanus) -25.2 -66.1 -38.2 -75.6 -26.6 -91.7 -38.2 -88.8
Northern Pintail (Anas acuta) -14.1 -36.3 -24.3 -40.3 -18.2 -49.7 -24.3 -52.0
American Pipit (Anthus rubescens) -38.1 -56.1 -30.3 -53.3 -34.0 -73.0 -29.4 -66.9
Woodhouse's Scrub-Jay (Aphelocoma woodhouseii) 5.8 38.4 21.8 27.2 23.1 23.6 23.7 -0.7
Golden Eagle (Aquila chrysaetos) -30.4 -42.6 -42.1 -55.4 -22.1 -68.0 -39.7 -73.4
Black-chinned Hummingbird (Archilochus alexandri) 0.4 4.1 -0.1 -0.9 0.1 -0.3 1.2 1.7
Great Blue Heron (Ardea herodias) 54.9 111.3 65.4 124.2 56.0 157.8 66.5 155.0
Western Cattle-Egret (Ardea ibis) -3.3 -4.4 -6.2 -5.2 -4.7 -3.0 -5.0 2.1
Sagebrush Sparrow (Artemisiospiza nevadensis) -50.3 -53.6 -60.1 -57.6 -40.1 -58.6 -57.5 -65.9
Short-eared Owl (Asio flammeus) -44.7 -74.9 -53.3 -73.9 -55.7 -84.6 -56.3 -83.2
American Goshawk (Astur atricapillus) 0.4 -2.6 2.9 2.1 -3.3 -4.1 2.7 8.6
Burrowing Owl (Athene cunicularia) 5.8 -5.4 -9.8 -8.6 0.5 -11.3 -10.1 -17.0
Juniper Titmouse (Baeolophus ridgwayi) 3.8 28.2 15.5 21.4 21.3 31.2 20.1 27.4
Upland Sandpiper (Bartramia longicauda) 13.7 19.4 34.7 29.1 14.6 30.6 33.3 38.5
American Bittern (Botaurus lentiginosus) -33.0 -38.0 -36.5 -46.1 -25.1 -54.6 -32.9 -59.1
Ferruginous Hawk (Buteo regalis) -48.9 -79.7 -60.6 -85.3 -49.5 -96.5 -60.4 -94.0
Swainson's Hawk (Buteo swainsoni) -34.9 -60.6 -45.1 -61.6 -42.0 -73.0 -45.1 -68.0
Lark Bunting (Calamospiza melanocorys) 21.6 29.4 21.9 33.7 17.9 37.6 20.3 34.5
Chestnut-collared Longspur (Calcarius ornatus) -70.1 -87.9 -76.2 -87.9 -74.7 -96.3 -77.7 -95.5
Canyon Wren (Catherpes mexicanus) 19.8 60.1 21.0 54.4 32.9 88.6 25.0 78.2
Greater Sage-Grouse (Centrocercus urophasianus) -35.4 -59.3 -38.7 -69.3 -21.6 -87.7 -35.5 -84.2
Baird's Sparrow (Centronyx bairdii) 20.0 4.8 18.0 16.6 2.2 9.0 11.2 10.6
Black Tern (Chlidonias niger) -33.8 -41.7 -33.9 -46.8 -28.0 -54.9 -32.2 -56.7
Common Nighthawk (Chordeiles minor) 31.7 87.1 41.4 98.5 38.9 126.2 42.6 122.8
Trumpeter Swan (Cygnus buccinator) -11.5 -33.9 -10.0 -26.2 -28.0 -59.7 -11.4 -40.9
Bobolink (Dolichonyx oryzivorus) 34.9 98.6 109.5 113.0 43.6 154.7 106.9 175.9
Snowy Egret (Egretta thula) -35.0 -34.1 -39.8 -44.4 -24.6 -48.7 -36.8 -50.6
Willow Flycatcher (Empidonax traillii) -8.3 -15.5 -15.1 -13.1 -18.4 -22.4 -13.3 -13.0
Merlin (Falco columbarius) -11.7 -20.5 -17.5 -24.1 -12.2 -35.5 -15.3 -32.7
Peregrine Falcon (Falco peregrinus) -22.9 -29.9 -29.6 -34.7 -21.6 -42.9 -28.5 -39.8
American Kestrel (Falco sparverius) -15.8 -26.5 -21.1 -32.7 -15.3 -45.5 -19.9 -44.9
Common Loon (Gavia immer) -7.0 -8.9 -2.1 -12.2 -5.1 -14.4 0.7 -5.9
MacGillivray's Warbler (Geothlypis tolmiei) 3.2 -0.3 3.7 0.3 -0.2 -5.2 3.5 -0.7
Common Yellowthroat (Geothlypis trichas) 67.6 121.7 76.5 132.3 66.6 160.6 77.9 155.1
Northern Pygmy-Owl (Glaucidium gnoma) -11.8 -28.5 -6.2 -26.2 -13.8 -49.7 -6.3 -38.3
Pinyon Jay (Gymnorhinus cyanocephalus) 47.0 113.8 55.5 120.1 63.0 155.5 58.2 147.9
Bald Eagle (Haliaeetus leucocephalus) 56.4 114.2 60.4 129.1 53.7 162.6 60.1 157.7
Evening Grosbeak (Hesperiphona vespertina) 18.8 22.3 16.4 28.1 15.3 19.6 19.0 26.1
Harlequin Duck (Histrionicus histrionicus) 9.6 -18.8 16.5 -11.1 -6.7 -47.2 17.1 -30.4
Caspian Tern (Hydroprogne caspia) 8.8 34.0 12.2 24.8 20.1 32.2 13.8 20.4
Loggerhead Shrike (Lanius ludovicianus) 4.9 -3.7 -15.0 -8.0 -0.1 -15.1 -16.4 -23.6
Virginia's Warbler (Leiothlypis virginiae) 17.9 35.4 18.2 34.9 16.3 63.2 21.4 69.1
Franklin's Gull (Leucophaeus pipixcan) -6.1 -4.5 -8.6 -4.7 -8.3 -8.8 -8.7 -9.9
Black Rosy-Finch (Leucosticte atrata) -33.0 -50.4 -25.7 -49.0 -29.1 -72.0 -25.8 -65.6
Brown-capped Rosy-Finch (Leucosticte australis) 15.2 100.2 7.9 78.1 92.7 12.2 13.2 12.0
Red Crossbill (Loxia curvirostra) 13.1 19.3 31.7 29.3 11.3 35.5 32.8 56.7
White-Winged Crossbill (Loxia leucoptera) -0.2 -4.7 6.5 1.2 -2.7 -5.5 7.5 0.8
Red-headed Woodpecker (Melanerpes erythrocephalus) 76.9 140.1 91.9 171.2 73.9 230.2 89.6 215.2
Lewis's Woodpecker (Melanerpes lewis) 15.4 13.5 13.4 11.7 3.4 13.7 12.9 11.7
Ash-throated Flycatcher (Myiarchus cinerascens) -8.6 32.4 2.3 7.6 30.7 4.8 12.0 -18.7
Clark's Nutcracker (Nucifraga columbiana) -10.9 -18.4 -9.3 -18.7 -9.0 -30.6 -7.9 -25.5
Long-billed Curlew (Numenius americanus) -35.2 -57.4 -39.6 -61.2 -39.0 -81.4 -40.6 -76.8
Black-crowned Night Heron (Nycticorax nycticorax) 22.2 47.5 12.2 52.4 25.7 55.5 13.0 41.8
Sage Thrasher (Oreoscoptes montanus) -52.9 -78.6 -59.3 -84.9 -44.6 -96.0 -57.6 -93.7
Blue Grosbeak (Passerina caerulea) 177.3 320.2 218.1 338.2 183.2 435.8 217.6 410.3
American White Pelican (Pelecanus erythrorhynchos) 44.8 113.9 38.4 121.2 50.5 162.1 40.7 142.3
Wilsons Phalarope (Phalaropus tricolor) -18.1 -26.3 -28.1 -29.7 -19.2 -35.7 -28.1 -39.7
Black-backed Woodpecker (Picoides arcticus) 61.7 78.9 53.9 79.6 35.4 116.2 53.8 122.3
White-faced Ibis (Plegadis chihi) -34.5 -41.3 -36.5 -48.3 -28.0 -56.6 -34.5 -57.1
Blue-gray Gnatcatcher (Polioptila caerulea) 26.7 27.7 16.8 27.8 24.3 32.7 17.4 25.2
Purple Martin (Progne subis) 51.4 45.0 53.6 57.3 14.6 56.1 52.1 65.4
Bushtit (Psaltriparus minimus) -8.3 -4.5 -5.6 -9.0 -2.9 -12.7 -5.0 -17.1
Flammulated Owl (Psiloscops flammeolus) 90.9 121.8 80.5 124.1 65.4 161.3 76.1 163.4
Virginia Rail (Rallus limicola) -4.3 -3.9 -5.3 -4.9 -3.5 -7.8 -4.8 -8.8
Thick-billed Longspur (Rhynchophanes mccownii) -67.2 -87.6 -73.1 -87.1 -72.7 -97.2 -74.6 -95.8
Calliope Hummingbird (Selasphorus calliope) 53.4 71.5 50.7 72.5 43.8 81.9 55.9 88.8
Rufous Hummingbird (Selasphorus rufus) 8.1 9.2 7.8 9.4 -0.1 12.9 7.9 16.4
Black-throated Gray Warbler (Setophaga nigrescens) -7.1 14.9 -10.6 0.1 16.1 9.2 -3.7 6.2
Pygmy Nuthatch (Sitta pygmaea) -4.9 2.3 -6.4 0.8 0.4 5.3 -5.2 -0.2
Williamson's Sapsucker (Sphyrapicus thyroideus) 9.0 -2.3 5.6 2.0 4.2 -25.2 4.3 -13.5
Dickcissel (Spiza americana) 65.3 123.9 90.1 146.9 68.1 195.2 90.0 194.9
Brewer's Sparrow (Spizella breweri) -41.5 -62.6 -49.5 -67.4 -38.5 -81.7 -47.8 -78.6
Field Sparrow (Spizella pusilla) -8.9 45.7 -7.8 52.4 0.2 70.1 -5.7 64.8
Forster's Tern (Sterna forsteri) -24.7 -22.3 -29.7 -32.5 -14.1 -35.3 -25.6 -42.2
Great Gray Owl (Strix nebulosa) 1.5 -4.6 2.2 -3.3 -0.2 -16.9 2.3 -9.3
Bewick's Wren (Thryomanes bewickii) -30.4 -44.6 -33.6 -53.4 -23.5 -65.7 -32.2 -67.3
American Barn Owl (Tyto furcata) 18.2 25.0 6.3 24.8 16.1 20.8 5.2 16.9
Red-eyed Vireo (Vireo olivaceus) 7.2 2.9 2.7 7.5 -0.8 -8.5 5.4 -5.7
Percent change (%)
1000%
500%
100%
0%
-100%

Figure 7.


MID-CENTURY
END-OF-CENTURY
MPI-ESM1-2-HR
GFDL-ESM4
MPI-ESM1-2-HR
GFDL-ESM4
Low
High
Low
High
Low
High
Low
High
Moose (Alces alces) -17.5 -34.5 -18.1 -31.4 -18.5 -59.0 -18.7 -47.1
Pallid Bat (Antrozous pallidus) 12.1 54.4 19.8 47.6 34.1 66.0 27.2 62.1
Townsend's Big-eared Bat (Corynorhinus townsendii) 68.0 127.4 86.0 140.8 72.7 183.9 86.6 178.6
White-tailed Prairie Dog (Cynomys leucurus) -38.0 -37.1 -43.3 -48.5 -22.2 -53.9 -39.9 -58.2
Black-tailed Prairie Dog (Cynomys ludovicianus) -3.3 -20.2 -29.3 -20.3 -12.5 -35.9 -32.3 -44.3
Spotted Bat (Euderma maculatum) 84.2 179.9 97.5 192.3 94.1 295.2 97.5 261.5
Northern Flying Squirrel (Glaucomys sabrinus) 70.7 105.4 76.2 111.0 60.4 142.9 76.7 152.7
Wolverine (Gulo gulo) 1.0 -12.8 14.0 -9.3 -2.7 -36.4 14.3 -22.7
Silver-haired Bat (Lasionycteris noctivagans) 13.9 21.2 15.9 22.0 12.6 28.7 16.6 34.5
Eastern Red Bat (Lasiurus borealis) 90.8 224.6 103.0 215.0 84.5 526.5 108.0 490.3
Sagebrush Vole (Lemmiscus curtatus) -60.9 -88.9 -68.3 -90.7 -65.0 -98.6 -70.3 -97.1
Northern River Otter (Lontra canadensis) -13.5 -22.1 -19.1 -19.7 -20.9 -35.4 -19.5 -31.6
Canada Lynx (Lynx canadensis) -32.0 -62.0 -24.1 -60.0 -33.8 -85.0 -25.0 -80.4
North American Water Vole (Microtus richardsoni) -54.4 -79.4 -41.6 -77.1 -48.1 -95.2 -40.2 -92.6
Western Small-footed Myotis (Myotis ciliolabrum) 0.4 12.8 4.3 7.1 10.3 9.3 7.3 7.6
Long-eared Myotis (Myotis evotis) 3.1 17.8 7.4 18.3 8.6 30.1 10.3 34.1
Little Brown Myotis (Myotis lucifugus) 5.5 25.9 13.0 23.1 14.8 34.2 16.5 36.4
Northern Myotis (Myotis septentrionalis) 29.9 52.2 57.0 61.0 29.0 69.1 57.1 80.2
Fringed Myotis (Myotis thysanodes) 40.1 76.0 58.2 82.6 36.3 121.8 60.7 149.5
Long-legged Myotis (Myotis volans) 24.8 75.4 37.5 78.1 38.3 121.2 41.6 119.7
Yuma Myotis (Myotis yumanensis) 22.2 79.6 34.2 66.8 45.6 102.4 45.1 104.4
Yellow-pine Chipmunk (Neotamias amoenus) 47.2 33.8 51.0 45.1 7.5 40.9 47.5 53.0
Cliff Chipmunk (Neotamias dorsalis) 8.6 -7.9 -1.2 -13.0 21.9 -10.8 -0.8 -4.7
Uinta Chipmunk (Neotamias umbrinus) -11.6 -30.6 -6.1 -22.3 -25.2 -42.5 -6.0 -30.0
American Pika (Ochotona princeps) -14.8 -32.9 -9.0 -29.9 -14.4 -61.8 -9.0 -50.7
Mule Deer (Odocoileus hemionus) 35.3 58.6 40.1 60.8 42.0 69.4 41.3 67.5
Bighorn Sheep (Ovis canadensis) -10.6 -17.4 -13.2 -19.4 -11.1 -29.4 -13.0 -28.5
Olive-backed Pocket Mouse (Perognathus fasciatus) 13.2 19.6 -4.3 12.7 14.3 14.6 -4.0 2.4
Pinon Deermouse (Peromyscus truei) 8.3 2.5 5.2 -3.7 14.3 -5.5 4.8 -3.6
Plains Harvest Mouse (Reithrodontomys montanus) 64.6 123.7 79.5 149.2 61.0 199.6 76.4 189.3
Western Spotted Skunk (Spilogale gracilis) 0.7 58.0 12.5 39.2 38.5 69.5 21.7 48.8
Plains Spotted Skunk (Spilogale interrupta) 0.1 -0.1 0.0 0.1 -0.2 0.1 0.0 0.2
Pygmy Rabbit (Sylvilagus idahoensis) -74.9 -92.5 -79.0 -94.4 -73.8 -99.4 -79.2 -98.3
Wyoming Pocket Gopher (Thomomys clusius) -77.9 -93.3 -82.3 -95.9 -78.8 -97.8 -82.5 -98.0
Swift Fox (Vulpes velox) -42.4 -52.3 -54.8 -55.9 -46.2 -63.9 -56.4 -69.1
Northern Meadow Jumping Mouse (Zapus hudsonius) 0.6 9.8 6.1 3.5 -11.4 42.5 5.3 30.0
Percent change (%)
1000%
500%
100%
0%
-100%

Figure 8.

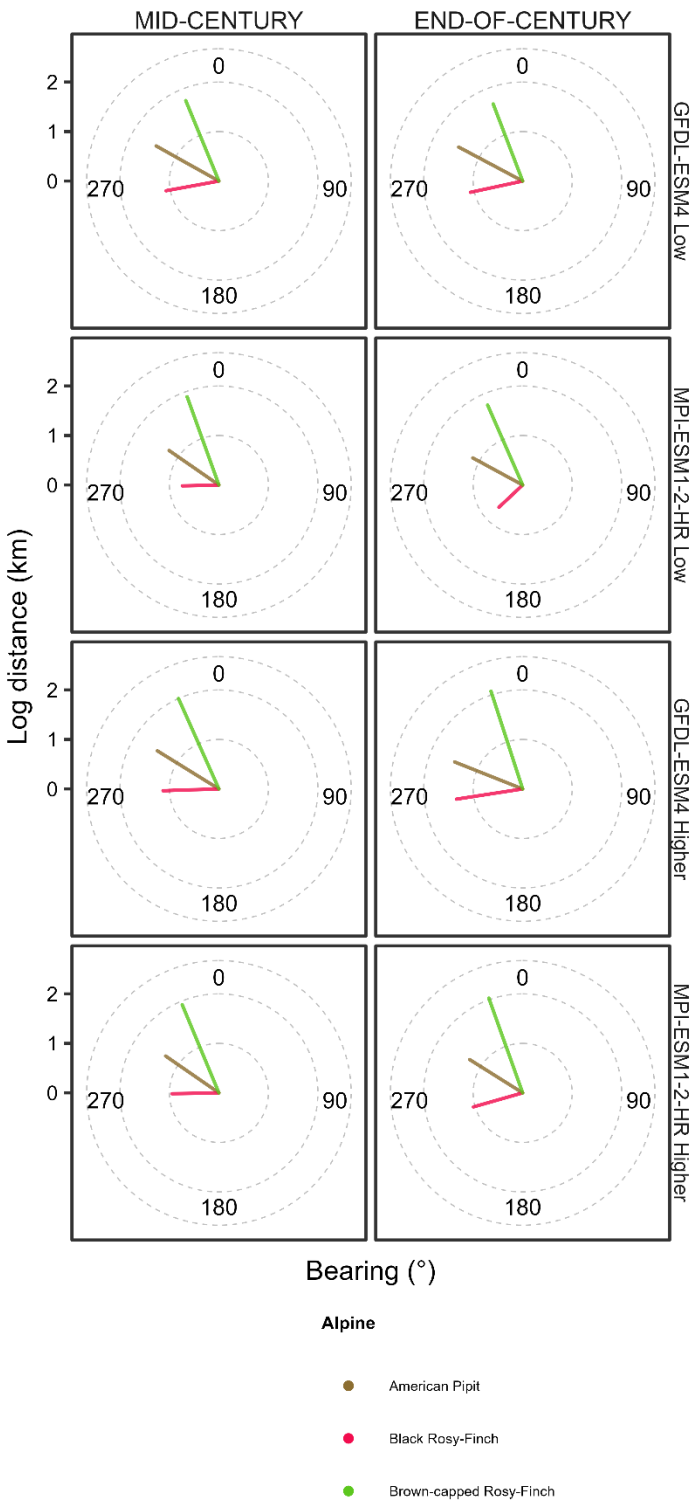
MID-CENTURY
END-OF-CENTURY
GFDL-ESM4 Low
MPI-ESM1-2-HR Low
GFDL-ESM4 Higher
MPI-ESM1-2-HR Higher
Log distance (km)
Bearing (°)
0
90
180
270
2
1
0
Alpine
American Pipit
Black Rosy-Finch
Brown-capped Rosy-Finch

Figure 9.

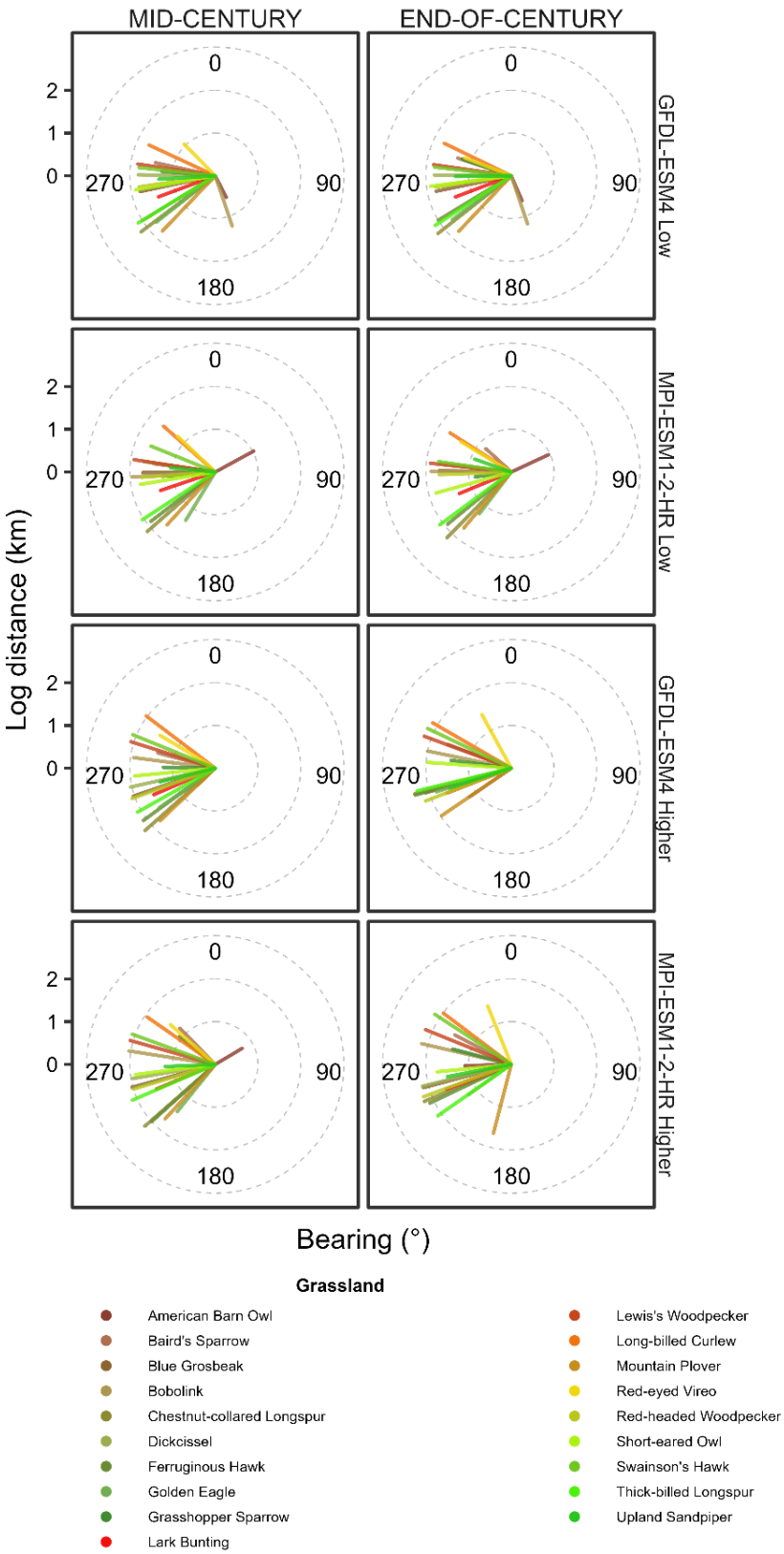
MID-CENTURY
END-OF-CENTURY
GFDL-ESM4 Low
MPI-ESM1-2-HR Low
GFDL-ESM4 Higher
MPI-ESM1-2-HR Higher
Log distance (km)
Bearing (°)
0
90
180
270
0
1
2
Grassland
American Barn Owl
Baird's Sparrow
Blue Grosbeak
Bobolink
Chestnut-collared Longspur
Dickcissel
Ferruginous Hawk
Golden Eagle
Grasshopper Sparrow
Lark Bunting
Lewis's Woodpecker
Long-billed Curlew
Mountain Plover
Red-eyed Vireo
Red-headed Woodpecker
Short-eared Owl
Swainson's Hawk
Thick-billed Longspur
Upland Sandpiper

Figure 10.

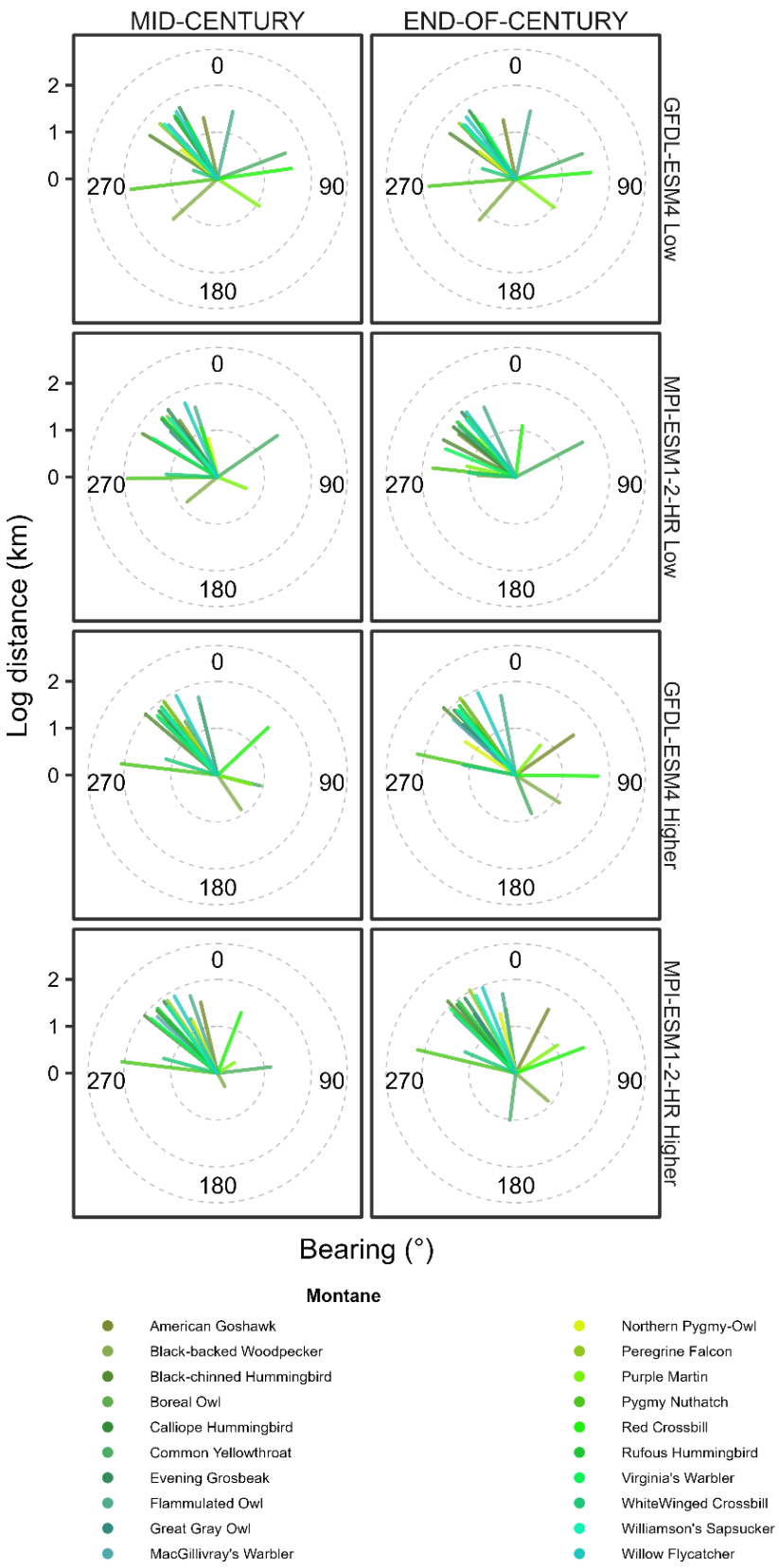
MID-CENTURY
END-OF-CENTURY
GFDL-ESM4 Low
MPI-ESM1-2-HR Low
GFDL-ESM4 Higher
MPI-ESM1-2-HR Higher
Log distance (km)
Bearing (°)
0
90
180
270
Montane
American Goshawk
Black-backed Woodpecker
Black-chinned Hummingbird
Boreal Owl
Calliope Hummingbird
Common Yellowthroat
Evening Grosbeak
Flammulated Owl
Great Gray Owl
MacGillivray's Warbler
Northern Pygmy-Owl
Peregrine Falcon
Purple Martin
Pygmy Nuthatch
Red Crossbill
Rufous Hummingbird
Virginia's Warbler
WhiteWinged Crossbill
Williamson's Sapsucker
Willow Flycatcher

Figure 11.

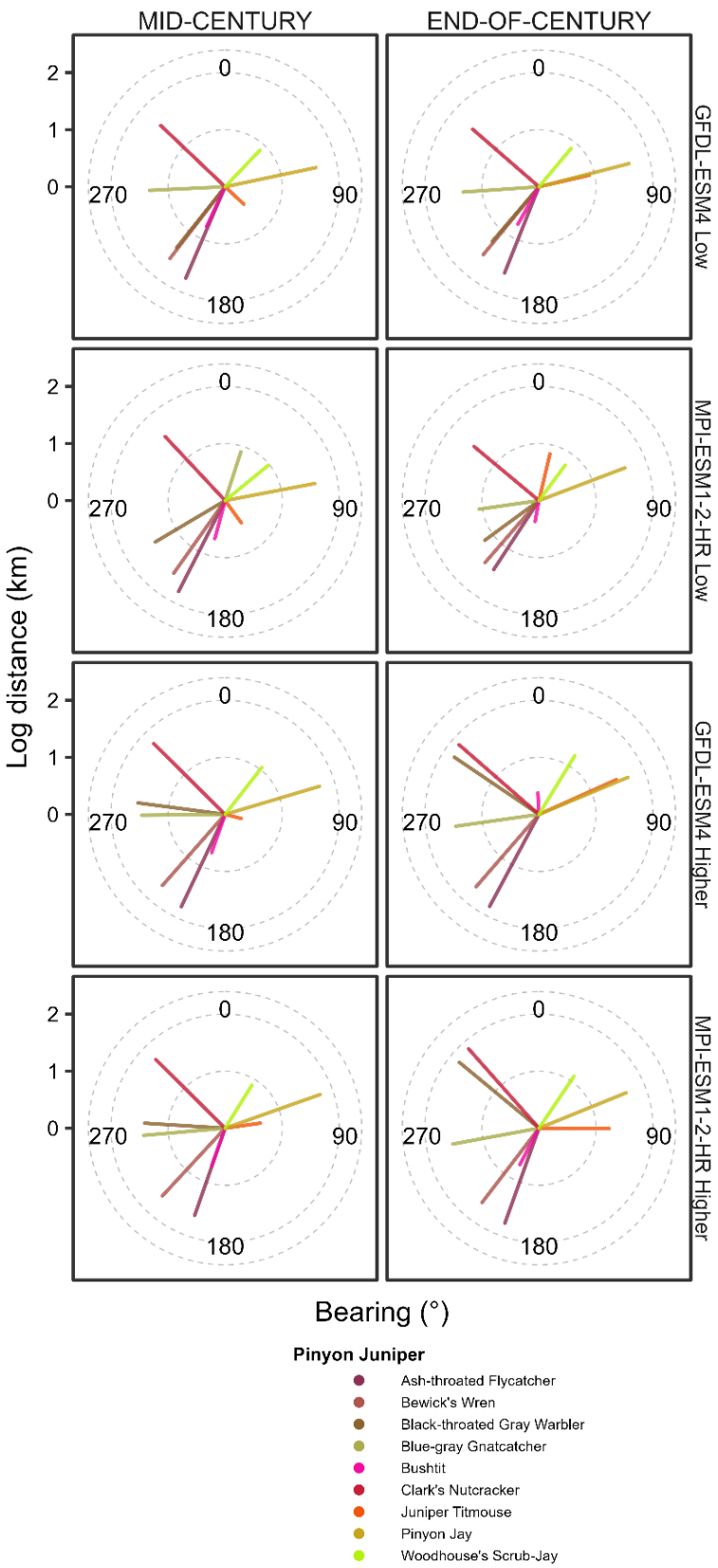
MID-CENTURY
END-OF-CENTURY
GFDL-ESM4 Low
MPI-ESM1-2-HR Low
GFDL-ESM4 Higher
MPI-ESM1-2-HR Higher
Log distance (km)
Bearing (°)
0
90
180
270
Pinyon Juniper
Ash-throated Flycatcher
Bewick's Wren
Black-throated Gray Warbler
Blue-gray Gnatcatcher
Bushtit
Clark's Nutcracker
Juniper Titmouse
Pinyon Jay
Woodhouse's Scrub-Jay

Figure 12.

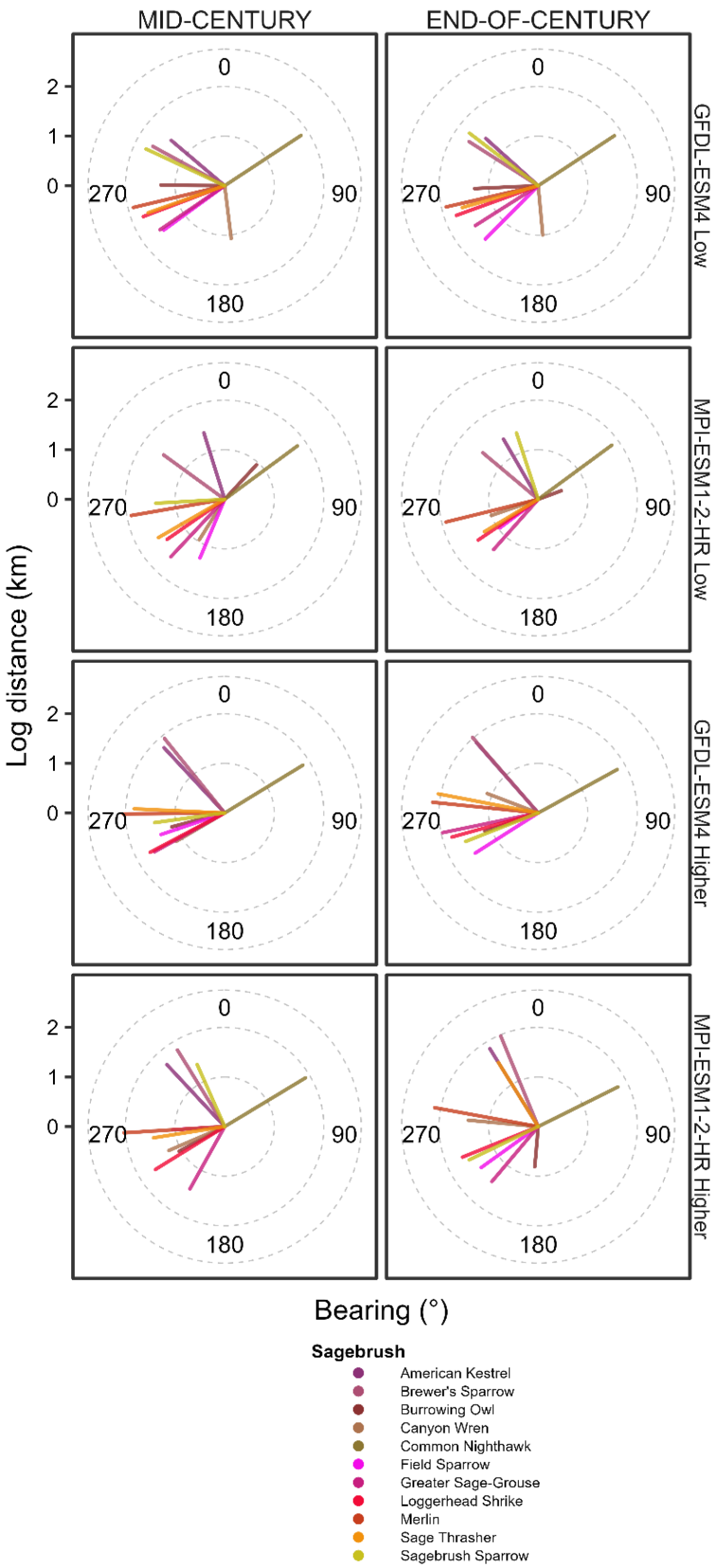
MID-CENTURY
END-OF-CENTURY
GFDL-ESM4 Low
MPI-ESM1-2-HR Low
GFDL-ESM4 Higher
MPI-ESM1-2-HR Higher
Log distance (km)
0
1
2
90
180
270
Bearing (°)
Sagebrush
American Kestrel
Brewer's Sparrow
Burrowing Owl
Canyon Wren
Common Nighthawk
Field Sparrow
Greater Sage-Grouse
Loggerhead Shrike
Merlin
Sage Thrasher
Sagebrush Sparrow

Figure 13.

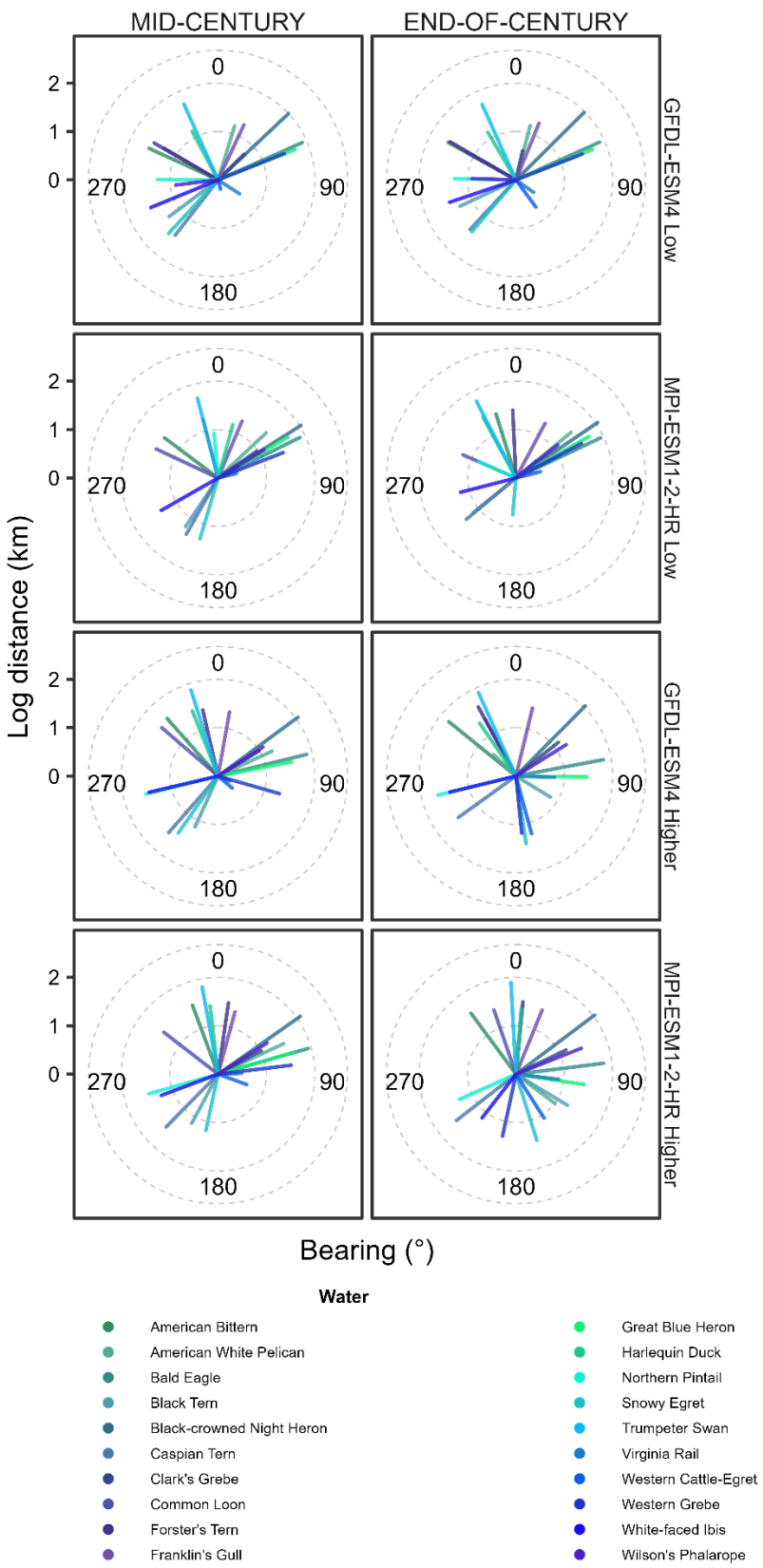
MID-CENTURY
END-OF-CENTURY
GFDL-ESM4 Low
MPI-ESM1-2-HR Low
GFDL-ESM4 Higher
MPI-ESM1-2-HR Higher
Log distance (km)
Bearing (°)
0
90
180
270
Water
American Bittern
American White Pelican
Bald Eagle
Black Tern
Black-crowned Night Heron
Caspian Tern
Clark's Grebe
Common Loon
Forster's Tern
Franklin's Gull
Great Blue Heron
Harlequin Duck
Northern Pintail
Snowy Egret
Trumpeter Swan
Virginia Rail
Western Cattle-Egret
Western Grebe
White-faced Ibis
Wilson's Phalarope

Figure 14.

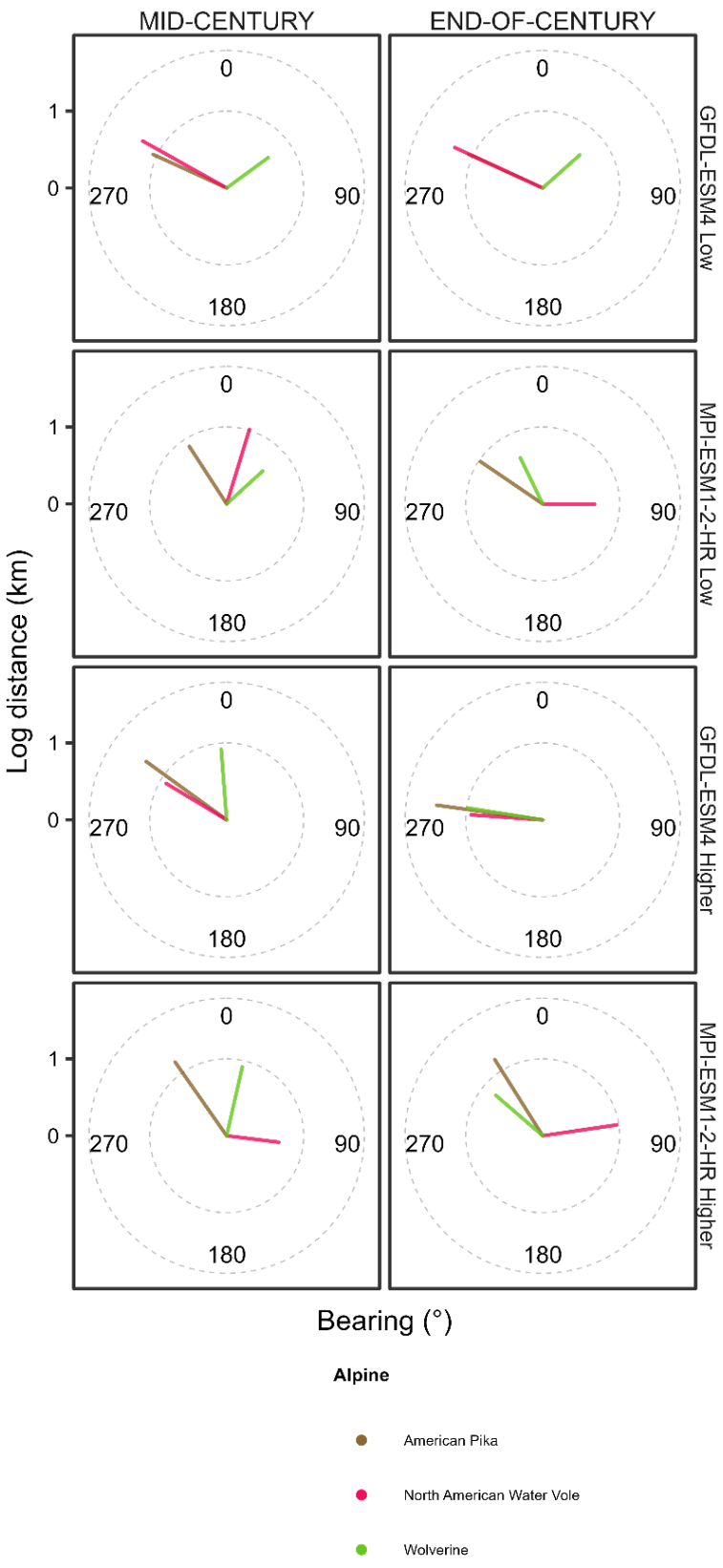
MID-CENTURY
END-OF-CENTURY
GFDL-ESM4 Low
MPI-ESM1-2-HR Low
GFDL-ESM4 Higher
MPI-ESM1-2-HR Higher
Log distance (km)
Bearing (°)
0
90
180
270
1
0
Alpine
American Pika
North American Water Vole
Wolverine

Figure 15.

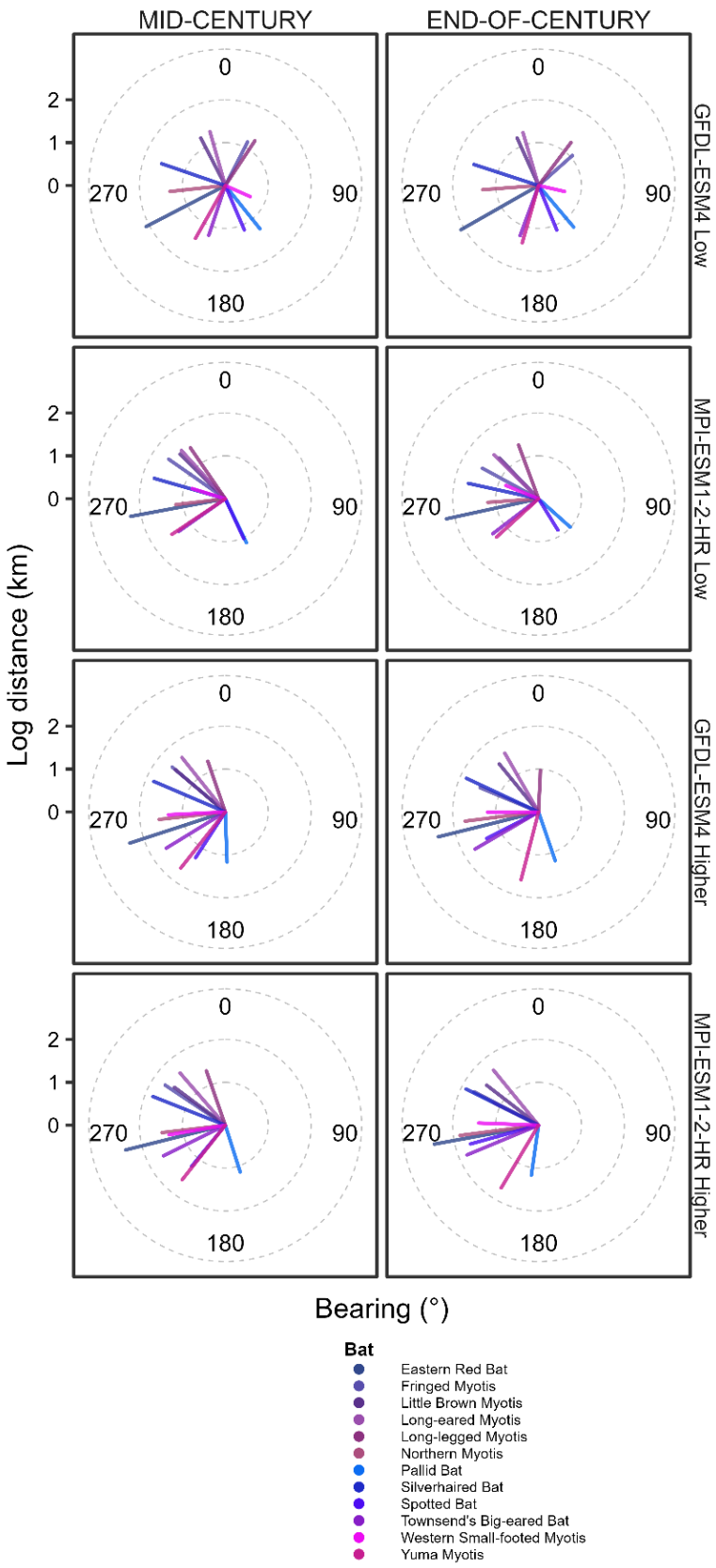
MID-CENTURY
END-OF-CENTURY
GFDL-ESM4 Low
MPI-ESM1-2-HR Low
GFDL-ESM4 Higher
MPI-ESM1-2-HR Higher
Log distance (km)
Bearing (°)
0
90
180
270
Bat
Eastern Red Bat
Fringed Myotis
Little Brown Myotis
Long-eared Myotis
Long-legged Myotis
Northern Myotis
Pallid Bat
Silverhaired Bat
Spotted Bat
Townsend's Big-eared Bat
Western Small-footed Myotis
Yuma Myotis

Figure 16.

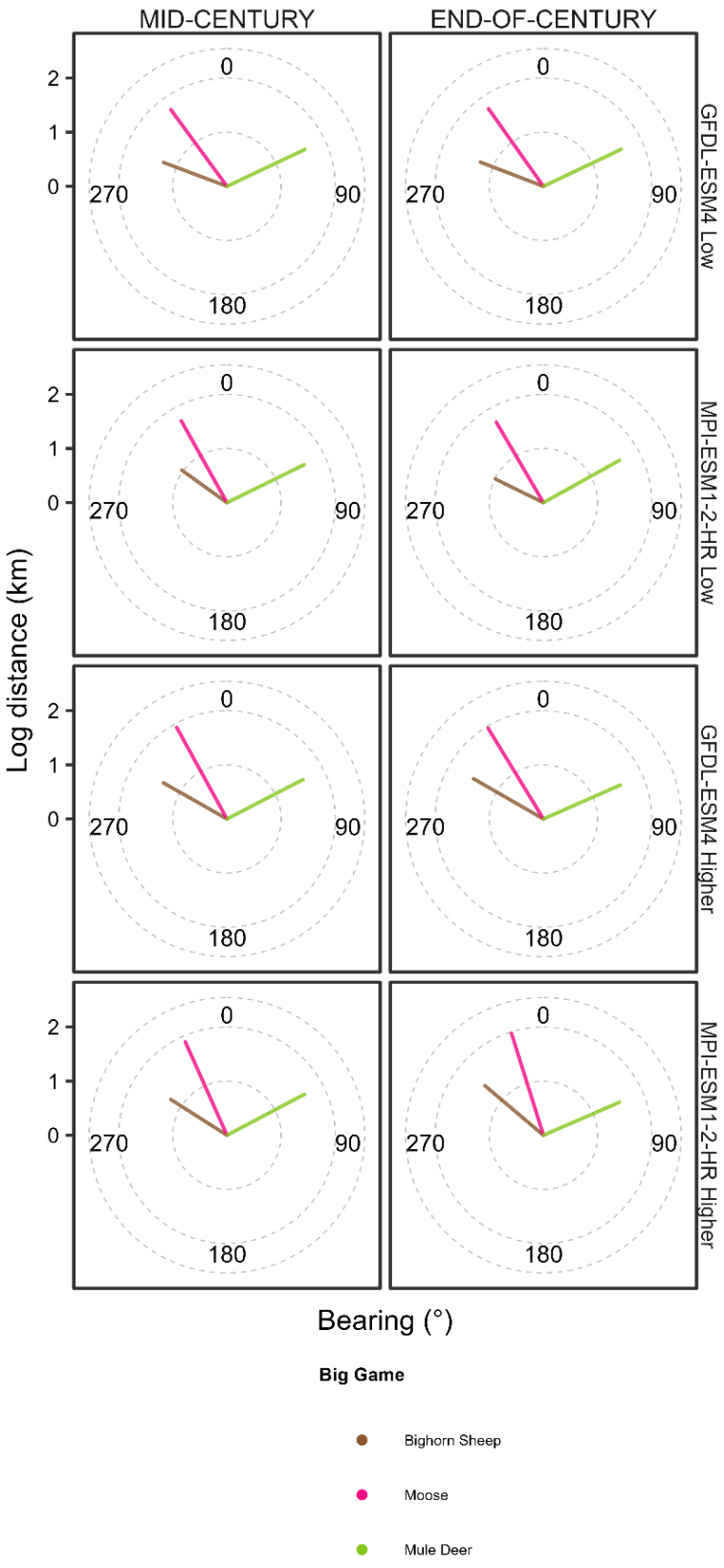
MID-CENTURY
END-OF-CENTURY
GFDL-ESM4 Low
MPI-ESM1-2-HR Low
GFDL-ESM4 Higher
MPI-ESM1-2-HR Higher
Log distance (km)
Bearing (°)
0
90
180
270
Big Game
Bighorn Sheep
Moose
Mule Deer

Figure 17.

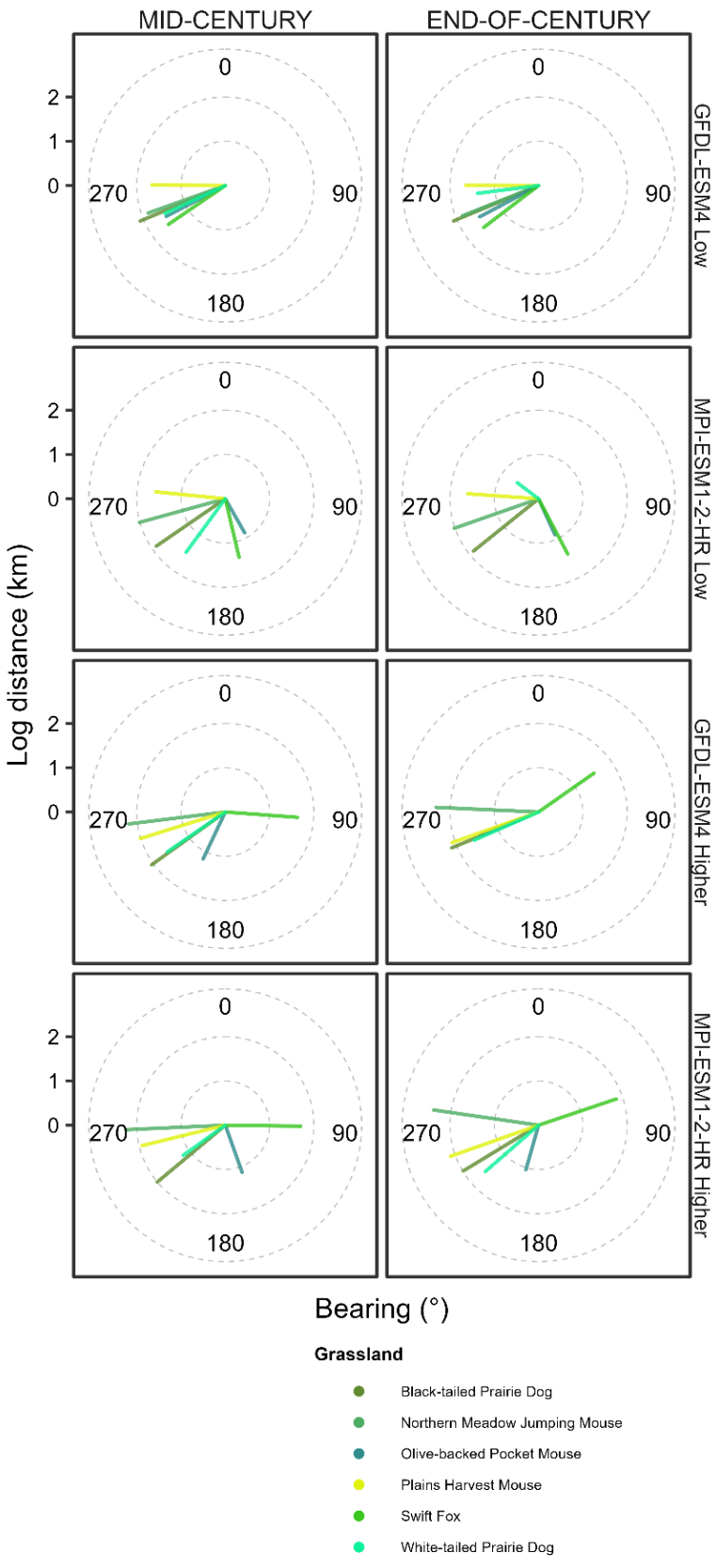
MID-CENTURY
END-OF-CENTURY
GFDL-ESM4 Low
MPI-ESM1-2-HR Low
GFDL-ESM4 Higher
MPI-ESM1-2-HR Higher
Log distance (km)
Bearing (°)
0
90
180
270
0
1
2
Grassland
Black-tailed Prairie Dog
Northern Meadow Jumping Mouse
Olive-backed Pocket Mouse
Plains Harvest Mouse
Swift Fox
White-tailed Prairie Dog

Figure 18.

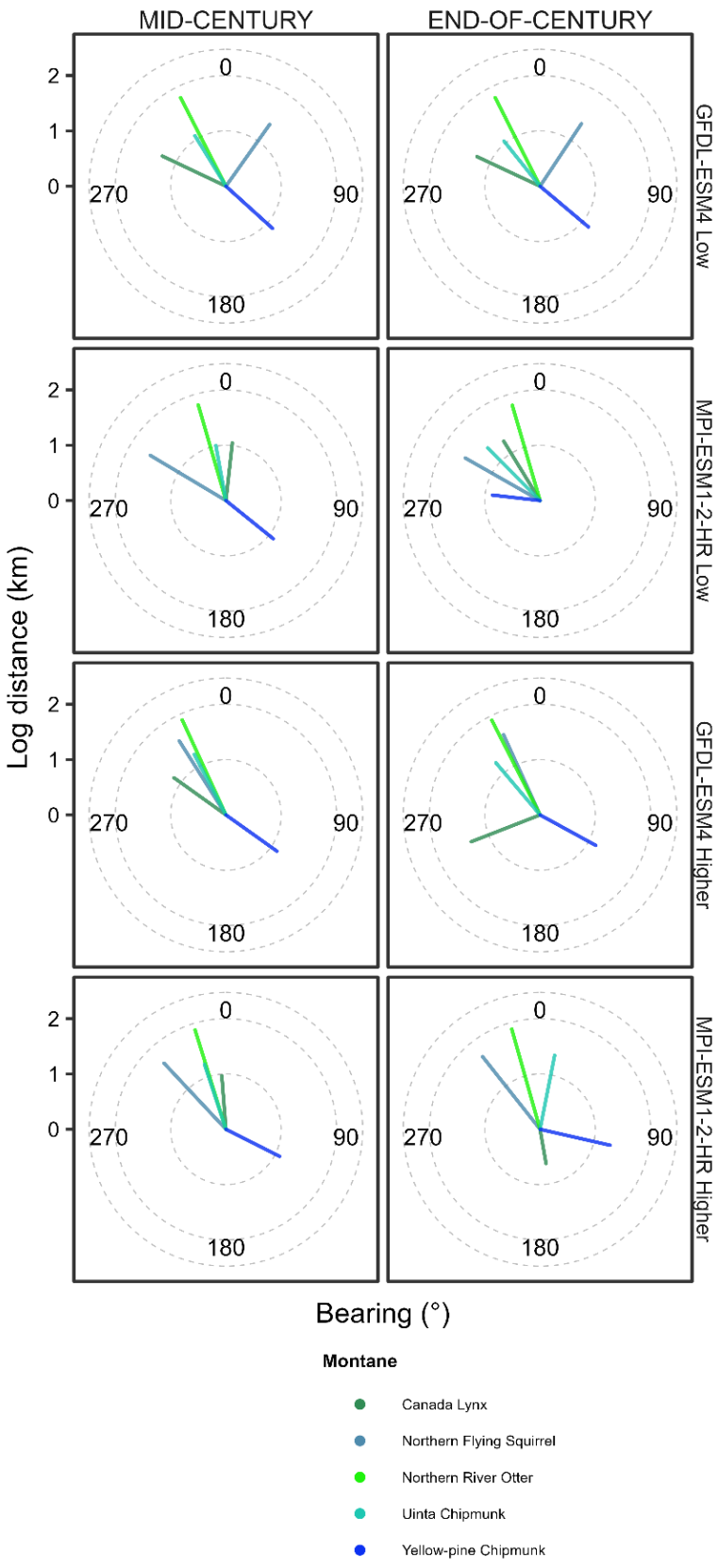
MID-CENTURY
END-OF-CENTURY
GFDL-ESM4 Low
MPI-ESM1-2-HR Low
GFDL-ESM4 Higher
MPI-ESM1-2-HR Higher
Log distance (km)
Bearing (°)
0
90
180
270
Montane
Canada Lynx
Northern Flying Squirrel
Northern River Otter
Uinta Chipmunk
Yellow-pine Chipmunk

Figure 19.

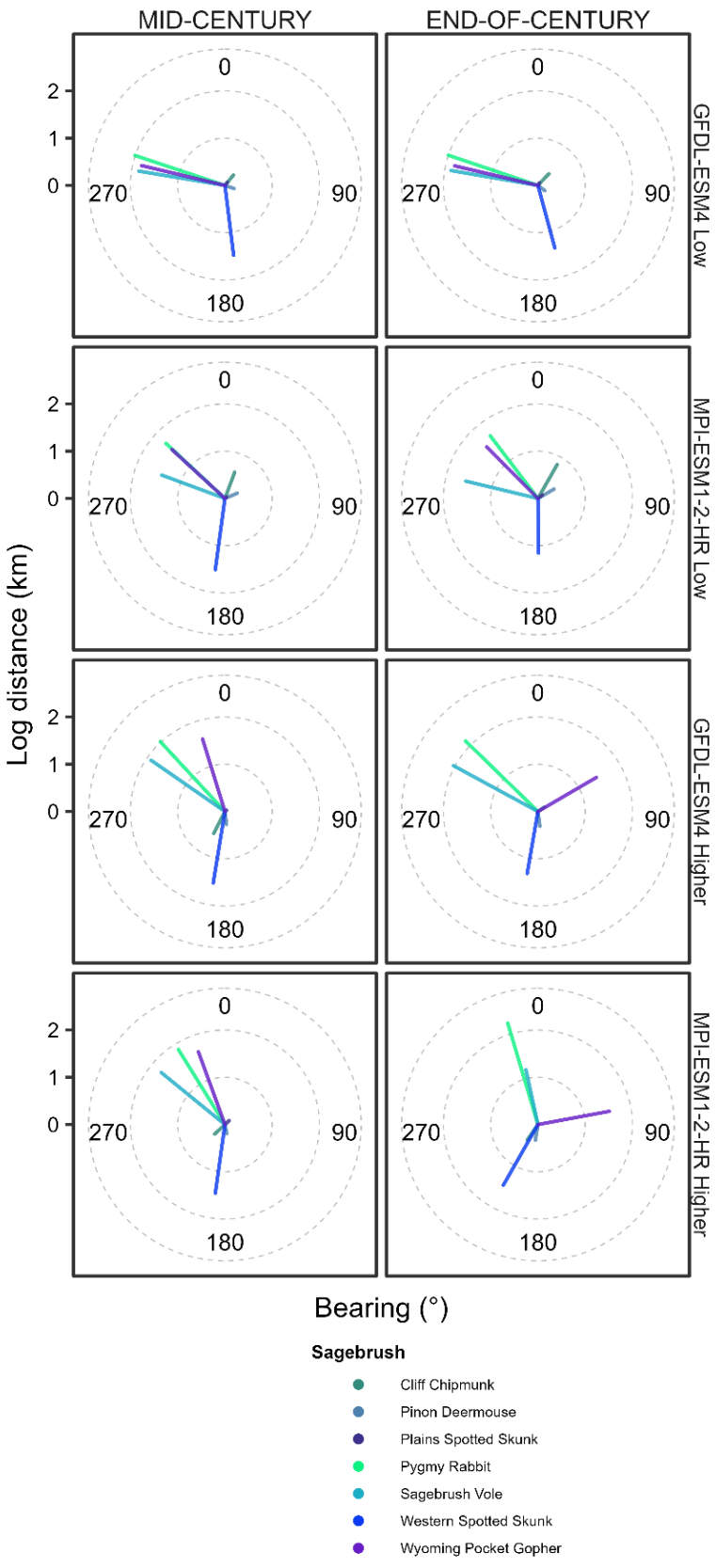
MID-CENTURY
END-OF-CENTURY
GFDL-ESM4 Low
MPI-ESM1-2-HR Low
GFDL-ESM4 Higher
MPI-ESM1-2-HR Higher
Log distance (km)
Bearing (°)
0
90
180
270
Sagebrush
Cliff Chipmunk
Pinon Deermouse
Plains Spotted Skunk
Pygmy Rabbit
Sagebrush Vole
Western Spotted Skunk
Wyoming Pocket Gopher

Figure 20.